สัญญาเลขที่ R2559B053

รายงานวิจัยฉบับสมบูรณ์

การก่อเกิดเฟส โครงสร้างจุลภาค และสมบัติทางไฟฟ้าของเซรามิกไพอิโซอิเล็กทริกระบบใหม่ (1-x)BNKLLT-xNKLNST ที่สังเคราะห์ด้วยเทคนิคการเผาไหม้

Phase formation, microstructure and electrical properties of new binary system of (1-x)BNKLLT-xNKLNST lead-free piezoelectric ceramics synthesized by the combustion technique

อ.ศุภรพรรณ ชูถิ่น
ผศ.ดร.ธีระชัย บงการณ์
ภาควิชาฟิสิกส์ คณะวิทยาศาสตร์ มหาวิทยาลัยนเรศวร

สนับสนุนโดยกองทุนวิจัยมหาวิทยาลัยนเรศวร

กิตติกรรมประกาศ

งานวิจัยนี้ได้รับการสนับสนุนงบประมาณจากงบประมาณแผ่นดินปี 2559 ผู้วิจัยและคณะขอขอบพระคุณ ณ โอกาสนี้

ขอขอบคุณเจ้าหน้าที่ภาควิชาฟิสิกส์ คณะวิทยาศาสตร์ มหาวิทยาลัยนเรศวร ทุกท่านซึ่งอำนวยความสะดวกเกี่ยวกับอุปกรณ์เครื่องมือต่างๆ

ขอขอบคุณ Science Lab Center คณะวิทยาศาสตร์ มหาวิทยาลัยนเรศวร ที่สนับสนุนเครื่องมือและอุปกรณ์ในการทำวิจัย

อ.ศุภรพรรณ ชูถิ่น และคณะ

Research Topic: Phase formation, microstructure and electrical properties of new binary system of (1-x)BNKLLT-xNKLNST lead-free piezoelectric ceramics synthesized by the combustion technique

Researcher: Miss.Suphornphun Chootin
Assist.Prof.Dr.Theerachai Bongkarn

ABSTRACT

The objective of this paper is to modify the piezoelectric properties of $Bi_{0.5}(Na_{0.68}K_{0.22}Li_{0.1})_{0.5}TiO_3$+ 0.10 wt% of La_2O_3 (BNKLLT) ceramics by the addition of $(K_{0.44}Na_{0.52}Li_{0.04})(Nb_{0.84}Ta_{0.10}Sb_{0.06})O_3$ (NKLNST) compound with forming solid state. Novel binary (1–x)BNKLLT–xNKLNST lead-free piezoelectric ceramics with an x content from 0 to 0.10 (step 0.02) were prepared via the solid state combustion technique with glycine used as the fuel. The affectation of x content on the structure evolution, morphology and electrical response of these ceramics were examined. The coexistence structure between rhombohedral and tetragonal was observed in the x = 0 sample. As x content increased between 0.02 and 0.04, the phase formation became a higher tetragonality structure. With x content ≥ 0.06, the phase formation began to change to a pseudo cubic phase. The microstructure exhibited a polyhedral grain shape in all samples. The average grain size of (1–x)BNKLLT–xNKLNST samples with various x content was in the same range (1.36-1.52 μm). The relative theoretical density increased from 96.7 to 97.2% when the NKLNST concentration was increased up to 0.04 and then decreased at higher concentrations. The reduction of T_{FA}, T_{SA} and the weak ferroelectric behaviour of these ceramics with increasing x content were observed. The resulting (1-x)BNKLLT–xNKLNST ceramics exhibited large piezoelectric coefficient of d_{33} up to 266 pC/N near the rhombohedral-tetragonal MPB at x = 0.04.

near morphotopic phase boundary (MPB) is a popular technique with interesting nowadays. C. Kornphom et al. [5] successfully fabricated high piezoelectric properties of (1-x)[$Bi_{0.5}(Na_{0.68}K_{0.22}Li_{0.1})_{0.5}TiO_3$+0.10 wt% of La_2O_3]-x[$(Ba_{0.90}Ca_{0.10})(Ti_{0.85}Zr_{0.15})O_3$] (x=0-0.1) (abbreviate to (1-x)BNKLLT-xBCTZ) binary system by solid state combustion technique, which the structure exhibited the coexisted phases of rhombohedral and tetragonal phase in all samples, where the highest d_{33} value about 295 pC/N was attained at x = 0.04 closed to MPB. In addition, many previous works indicated that introducing KNN-based compound into BNT-based ceramics can improve the density and electrical behavior which is of great interest at this time [15, 16].

For this reason, we tested the idea of the addition of $(K_{0.44}Na_{0.52}Li_{0.04})(Nb_{0.84}Ta_{0.10}Sb_{0.06})O_3$ (KNLNST) ceramics with large piezoelectric constant (350-450 pC/N) [17, 18] into BNKLLT ceramics to form a new solid solution in order to increase the piezoelectric properties of BNKLLT. From a literature review, the investigation and preparation of (1-x)BNKLLT-xKNLNST ceramics ($0 \leq x \leq 0.10$) by the solid state combustion technique has not been studied up until now. So, in this work, the goal was to design a new binary solid solution of (1-x)BNKLLT-xNKLNST with $0 \leq x \leq 0.10$ prepared by the solid state combustion technique. The effect of NKLNST content on the phase evolution, microstructure and electrical properties were investigated.

Objectives of this research

The objectives of this research are as follow:

1. To prepare (1-x)BNKLLT-xKNLNST ceramics ($0 \leq x \leq 0.10$) using the solid state combustion technique.

2. To investigated the optimum calcination and sintering conditions of (1-x)BNKLLT-xKNLNST ceramics ($0 \leq x \leq 0.10$) by the solid state combustion technique.

3. To study the effect of calcination and sintering temperatures on phase formation, microstructure and electrical properties of (1-x)BNKLLT-xKNLNST ceramics ($0 \leq x \leq 0.10$) by the solid state combustion technique.

Expected outputs of the study

1. To obtain information on the preparation of (1-x)BNKLLT-xKNLNST ceramics ($0 \leq x \leq 0.10$) using the solid state combustion technique.

2. To obtain information on the optimum calcination and sintering conditions of (1-x)BNKLLT-xKNLNST ceramics ($0 \leq x \leq 0.10$) by the solid state combustion technique.

3. To understand the effect of calcination and sintering temperatures on phase formation, microstructure and electrical properties of (1-x)BNKLLT-xKNLNST ceramics ($0 \leq x \leq 0.10$) prepared by the solid state combustion technique.

CHAPTER II

THEORY AND LITERATURE

This chapter contains details on the brief description of necessary concepts of the perovskite ferroelectrics. In addition, the relevant literatures on processing and characteristics of both powders and ceramics are reviewed with attention paid on their properties.

Perovskite Structure

Since the ferroelectric properties of barium titanate were reported by Von Hippel in 1945, ABO_3 compound with the perovskite structure have been studied extensively. These studies have resulted in the discovery of many new ferroelectric and piezoelectric materials. Most of the literatures on perovskite-type compounds have concentrated on these properties.

Perovskite structure is a crystal structure of a mineral perovskite calcium titanate ($CaTiO_3$) which was discovered by Count Lev Aleksevich von Perovski [30]. This structure is adopted by many oxides that the general chemical formula of ABO_3. The general crystal structure is a primitive cube which the A represents a cation with larger ionic radius in the corner, B represents a cation with a smaller ionic radius in the middle of the cube and O is oxygen in the centre of the face edges. Figure 1 shows a cubic perovskite structure unit cell (a) and three-dimensional network of BO_6 octahedra (b). The sites are occupied by Ba^{2+}, Pb^{2+}, K^+ or Na^+ ions, and B sites by Ti^{4+}, Zr^{4+}, Nb^{5+} or Ta^{5+} ions. Some examples of perovskite-type ceramic compounds are lead titanate ($PbTiO_3$), barium titanate ($BaTiO_3$), bismuth sodium titanate ($Bi_xNa_{1-x}TiO_3$), potassium niobate ($KNbO_3$), etc. The perovskite structure can tolerate a wide range of compositional variation. Thus, its properties are differed behavior [29, 31, 32].

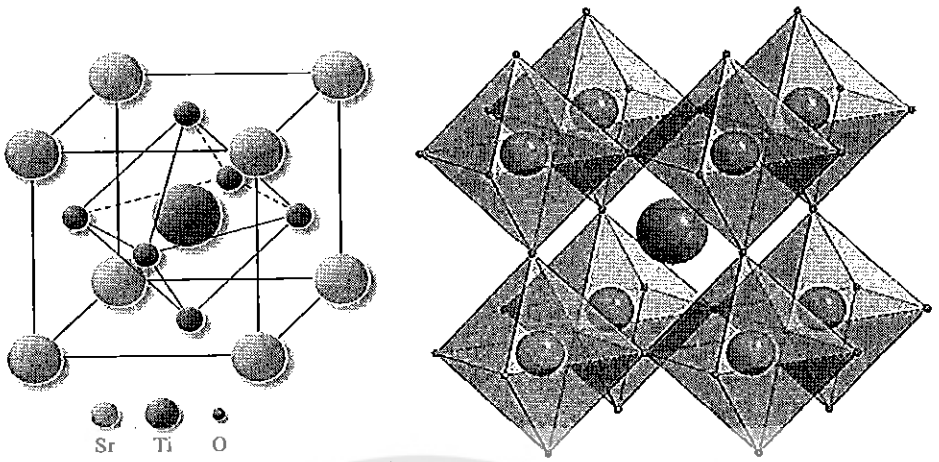

Figure 1 (a) A cubic $SrTiO_3$ perovskite-type unit cell and (b) three-dimensional network of BO_6 octahedra [26]

Piezoelectricity

Piezoelectricity was discovered in 1880 by Jacques and Pierre Curie during their systematic study of the effect of pressure on the generation of a electrical charge by crystals such as quartz, zincblend, and tourmaline [32]. The name "piezo" is derived from the Greek, meaning "to press", hence piezoelectricity is the generation of electricity as a result of mechanical pressure. Many piezoelectric materials are not ferroelectric but all ferroelectrics are piezoelectric. Two effects are operative in piezoelectricity. The direct effect is identified with the phenomenon whereby an electrical charge (polarization) is generated from mechanical stress, whereas the converse effect is associated with the mechanical movement generated by the application of an electrical field. Both of these effects are illustrated in Figure 2.

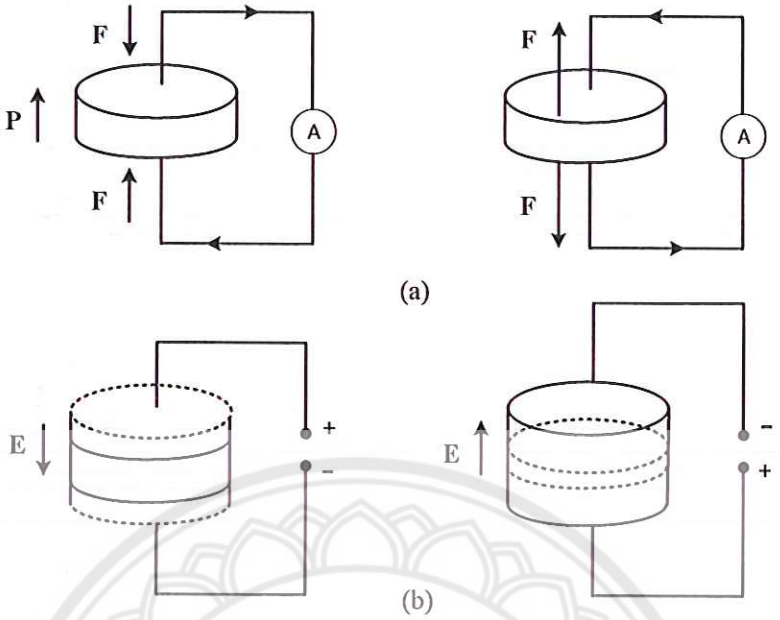

Figure 2 Piezoelectric effects in ferroelectric ceramics
(a) direct effect (b) converse effect [32]

The basic equations that describe these two effects in regard to electric and elastic properties are

$$D = dT + \varepsilon^T E \quad (1)$$

$$S = s^E T + dE \quad (2)$$

Where D is the dielectric displacement (consider it equal to polarization), T the stress, E the electric field, S the strain, d a piezoelectric coefficient, s the material compliance (inverse of modulus of elasticity), and ε the dielectric constant (permittivity). The subscripts indicate a quantity held constant: in the case of ε^T, the stress is held constant, which means that the piezoelectric element is mechanically unconstrained, and, in the case of s^E, the electric field is held constant, which means the electrodes on the element are shorted together.

Ferroelectrics

Ferroelectricity is a phenomenon which was discovered by Valasek in 1921 [33]. It has become customary to call ferroelectricity the phenomenon exhibited by these crystals and ferroelectric the crystal themselves. This is due to a formal similarity of the ferroelectric phenomenon with that of ferromagnetism. The similarity is mainly phenomenological. As ferromagnetic materials exhibit a spontaneous magnetization and hysteresis effects in the relationship between magnetization and magnetic field, ferroelectric crystals show a spontaneous electric polarization and hysteresis effects in the relation between the dielectric displacement and the electric field. This behavior is mostly observed in certain temperature regions below by transition temperature (Curie temperature) where those crystals above are this transition temperature are no longer ferroelectric.

The crystal symmetries of the paraelectric and ferroelectric phase are an important factor in displaying the ferroelectric behavior of the materials. The lattice structure described by the Bravais unit cell of the crystal governs the crystal symmetry. Though there are thousands of crystals in nature, they all can be grouped together into 230 microscopic symmetry types or space groups based on symmetry elements. It can be shown by the inspection of the 230 space groups that there are just 32 point groups. As shown in Figure 3, the 32 point groups can be further classified into (a) crystal having a center of symmetry and (b) crystals which do not possess a center of symmetry (noncentrosymmetric). There are 21 classes of noncentrosymmetric, a necessary condition for piezoelectricity to exist, and only 20 are piezoelectric. Among these 20 point groups, only 10 can display a spontaneous polarization, which is designated as pyroelectric. A subgroup of the spontaneous polarized pyroelectric is a category of materials known as ferroelectrics. Ferroelectrics are a special class of materials in which a permanent electric dipole can be reoriented between equilibrium states by the external electric field. Continuing Valasek's analogy between ferroelectric and ferromagnetic, the dependence of the polarization on an applied electric field can be seen by polarization versus electric field i.e. (P-E) hysteresis loop as shown in Figure 4. The hysteresis loop is typically observed using the simple circuit described by Sawyer-Tower [34]. One parameters obtained from the hysteresis loop measurement, the remnant polarization (P_r) is the crystal spontaneous

polarizes along one of the allowed direction without applied electric field. The field required to reverse the polarization is known as the coercive field (E_c).

Normal ferroelectric materials have a sharp phase transition which occurs at a specific temperature called the Curie temperature, T_c. The T_c is the temperature which the crystal structure transforms from the paraelectric state into the ferroelectric state and vice versa [29, 35, 32]. In the paraelectric state, the dielectric permittivity obeys the Curie-Weiss law.

$$\varepsilon_r = \frac{C}{T - T_0} \tag{3}$$

Where C is the Curie-Weiss constant, T is the temperature and T_0 is the Curie-Weiss temperature. The Curie temperature (T_c) and the Curie-Weiss temperature (T_0) should not be confused. The Curie temperature is the actual transformation temperature, but the Curie-Weiss temperature is found by extrapolating the plot of the Curie-Weiss law, as shown in Figure 5. The Curie temperature and Curie-Weiss temperature typically differ by only a small amount that depends on the type of phase formation the material undergoes. The Curie-Weiss temperature can be as much as ten degrees lower than the Curie temperature for first-order phase transformations and the two can be nearly equal for second-order phase transformations (first order phase transformations are those in which the first derivative of the free energy, with respect to temperature, is discontinuous; second order phase transitions are those in which the second derivative is discontinuous).

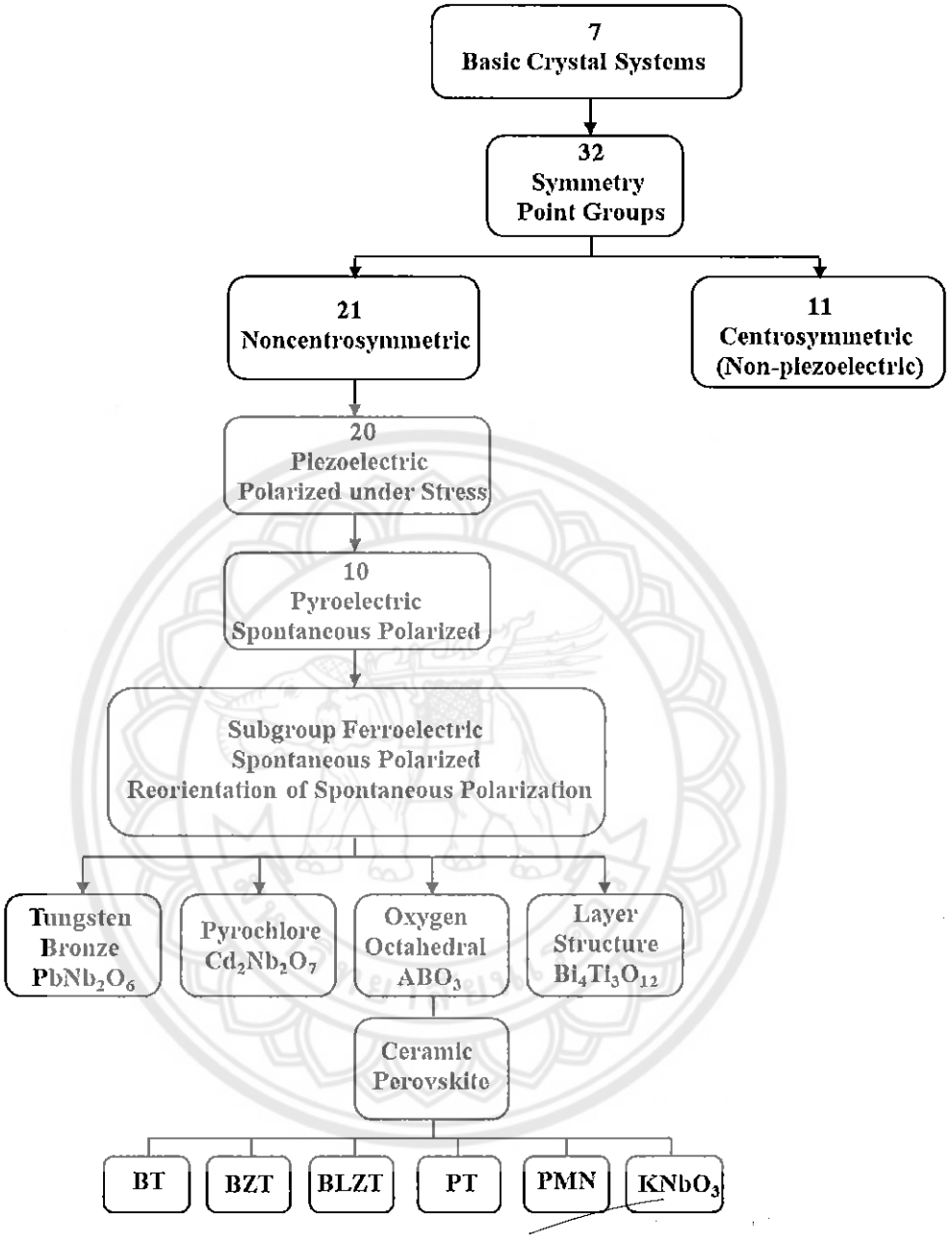

Figure 3 Interrelationship of piezoelectric and subgroups on the basis of symmetry [31]

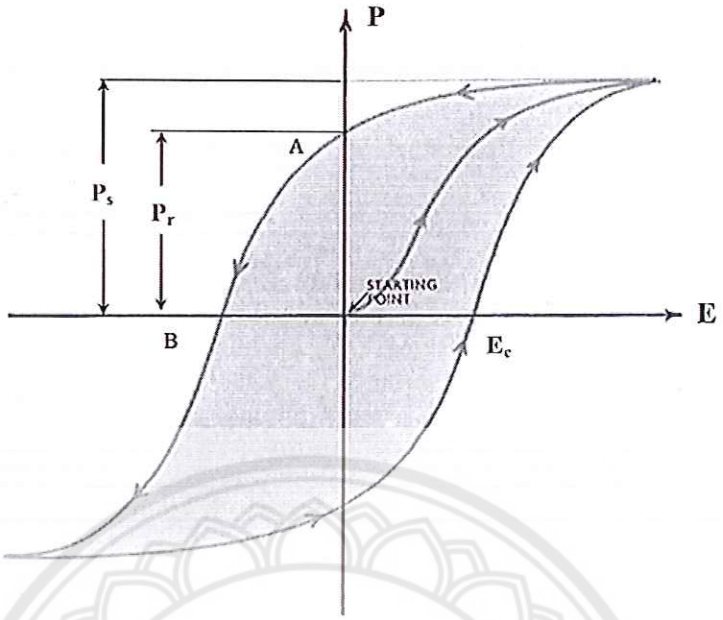

Figure 4 A ferroelectric hysteresis loop [34]

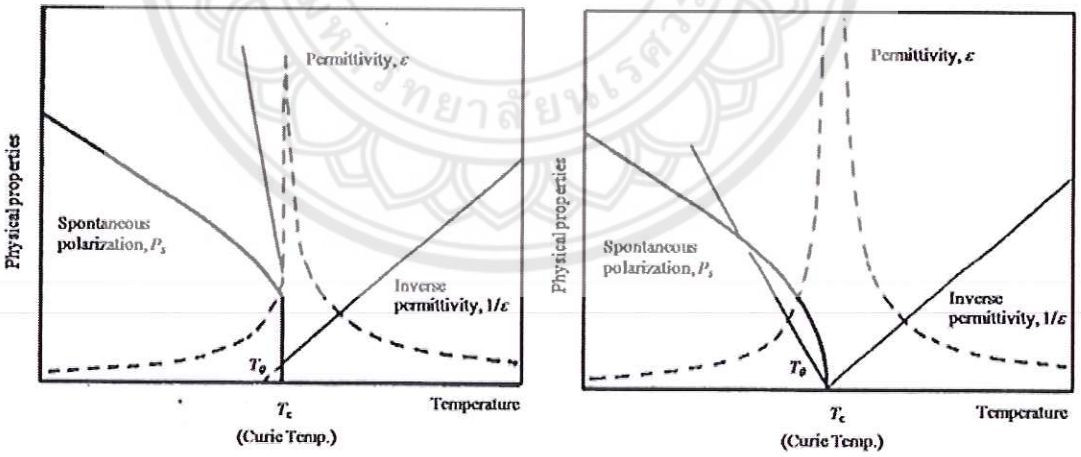

Figure 5 Phase transition in a ferroelectric (a) first order and (b) second order [35]

Antiferroelectric

An antiferroelectric crystal is defined as a crystal whose structure can be considered as being composed of two sublattices polarized spontaneously in antiparallel directions and in which a ferroelectric phase can be induced by applying an electric field. Experimentally, the reversal of the spontaneous polarization in ferroelectrics is observed as a single hysteresis loop, and the induced phase transition in antiferroelectrics as a double hysteresis loop (Figure 6), when a low-frequency ac field of a suitable strength is applied [37].

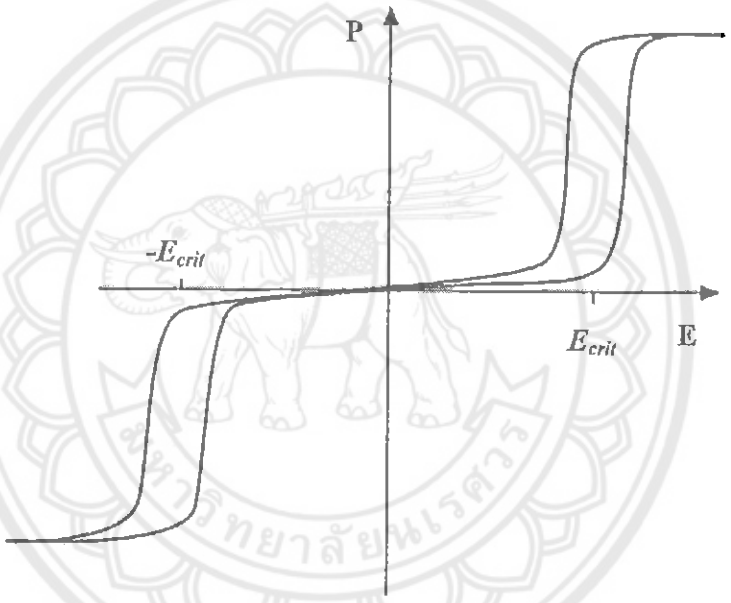

Figure 6 Antiferroelectric hysteresis loop [37]

Paraelectric

Paraelectricity is the ability of many materials (specifically ceramic crystals) to become polarized under an applied electric field. Unlike Ferroelectricity; this can happen even if there is no permanent electric dipole that exists in the material, and removal of the fields results in the polarization in the material returning to zero, as shown in Figure 7. The mechanisms which give rise to paraelectric behavior are the distortion of individual ions (displacement of the electron cloud from the nucleus) and the polarization of molecules or combinations of ions or defects. Paraelectricity occurs in crystal phases in which electric dipoles are unaligned (i.e. unordered

domains that are electrically charged) and thus have the potential to align in an external electric field and strengthen it. In comparison to the ferroelectric phase, the domains are unordered and the internal field is weak. The $LiNbO_3$ crystal is ferroelectric below 1430 K, and above this temperature it turns to paraelectric phase. Other perovskites similarly exhibit paraelectricity at high temperatures [38].

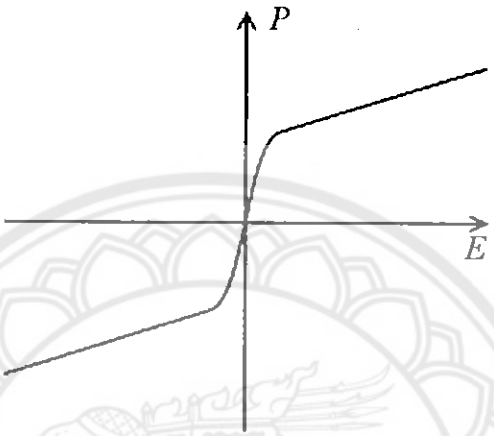

Figure 7 Paraelectric hysteresis loop [38]

Typical methods to synthesize ceramics

Solid-state reaction method

Solid-state reaction method is the most widely used method for the preparation of polycrystalline solids from a mixture of solid starting materials. This method involves chemical decomposition, where solid reactants are heated to produce a new solid and normally use simple oxides powders such as carbonates, hydroxides, nitrates, sulfates, acetates, oxalates, alkoxides and other metal salts for preparation. The solids do not react together at room temperature over normal time scales and it is necessary to heat them to much higher temperatures, often to 1000 to 1500 °C in order for the reaction to occur at an appreciable rate. An example of reaction between barium carbonate and titanium oxide at high temperature produce barium titanate by using solid-state reaction method.

$$BaCO_3(s) + TiO_2(s) \text{ -- (~1200 °C) -----> } BaTiO_3(s) + CO_2\ (g) \qquad (4)$$

Solid-state reactions generally have an advantage in terms of production cost. However, it is commonly understood that the conventional solid state method requires compulsory grinding of different oxide mixtures for long periods of time as well as sintering. In addition, the synthesized component distributions are not homogeneous and particle sizes are relatively large [39, 40].

Sol-gel processing

Sol-gel process is a method for producing solid materials from small moleculesin a solution (sols) agglomerate and under controlled conditions eventually link together to form a coherent network (gel). The method is used for many applications in synthesis of novel materials. The advantages of the sol-gel process in general are high purity, homogeneity and low temperature. For a lower temperature process, there is a reduced loss of volatile components are thus the process is more environmental friendly. In addition, some materials that cannot be made by conventional means because of thermal and thermodynamically instability can be made by this process. However, the disadvantages are also real. The starting materials can be fairly expensive [41, 42].

Co-precipitation method

Co-precipitation (CPT) is the carrying down by a precipitate of substances normally soluble under the conditions employed. This method proceeds in two stages. First stage, the impurity is trapped either on the surface or inside the growing particles. If the growing particles have a crystal structure, then the impurity will become localized at regions of the solid phase with a perfect structure. During rapid precipitation, the growing particles will trap non-equilibrium impurities, which are usually in homogeneously distributed through the volume of the solid phase. In the second stage, the concentration of defects within the precipitate decrease and the particles are flocculated. Impurities trapped during the first stage return either partially or completely to the medium. The concentration of impurities in the solid phase becomes equalized. The crystals acquire an equilibrium composition that depends only on the composition and temperature of medium [41, 42].

Combustion method

Combustion method is the method based on the principle that once a reaction is initiated under heating, an exothermic reaction occurs from the oxidation-reduction reaction between reaction materials and fuel. It has emerged as an important technique for the synthesis and processing of advanced ceramics, which involves a self-sustained reaction. The advantages of this technique include inexpensive raw materials, simple and fast preparation process, fine powders with high homogeneity and low firing temperature and shorter dwell time [43, 44, 45, 46]. The advantages of this method over other combustion methods are: firstly, being a solution process, it has control over the homogeneity and stoichiometry of the products; secondly, it is possible to incorporate desired impurity ions in oxide hosts and prepare industrially useful materials; thirdly, the process is simple and fast. Moreover, in fact, the reaction mechanism of this method is very complex due to there are several parameters influencing the reaction such as the type of fuel, fuel-oxidizer ratio, etc [47].

The fuel that used in combustion method was commonly an organic compound. Generally, a good fuel should reacted nonviolent, produce nontoxic gases, also acts as a chelating material for metal cations. It serve two purposes; first for the source of C and H which on combustion form CO_2 and H_2O and liberate heat and second for forming complexes with the metal ions facilitating homogeneous mixing of cations in solution. The nature of fuel and its amount are some of the important process parameter that influencing on the powder characteristics like a crystallite size, surface area nature of agglomeration, etc. The several fuels were used in the combustion method, e.g., urea, glycine, citric acid, alanine, carbohydrazide, poly acrylic acid, oxalic acid, acetyl acetone, metal acetate, hydrazine. Thus, the selection of an appropriate fuel is very important for the combustion system. Some properties of organic compounds used in combustion synthesis method are shown in Table 1. The commonly used fuels are; glycine, citric acid and urea. They were described as below;

1. Glycine

Glycine is one of the cheapest amino acids and is known to act as a complexing agent for a large amount of metallic ions. The glycine molecule has a carboxylic acid group located at one end of the chain and an amino group.

2. Citric acid

Citric acid is a weak organic acid that act as a convenient ligand which is inexpensive and is a more effective complexing agent for metal ions. The structure consists of three carboxyl groups and a hydroxyl group.

3. Urea

Urea is an attractive fuel for originating the formation of powders with crystallite sizes in the submicron/nanosized range and act as a complexing agent for metal ions because it contains two amino groups located at the extremes of its chemical structure.

Table 1 Some properties of organic compounds [48]

Properties	Organic component				
	Alanine	Glycine	Carbohydrazide	Urea	Citric acid
Structure formula	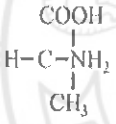	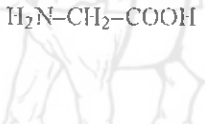	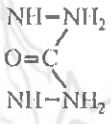	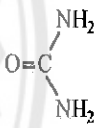	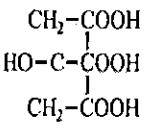
Molecular weight (g/mol)	80.1	90.1	75.1	60.1	192.1
Heat of combustion (kJ/g)	18.2	13.0	12.6	10.5	10.2
Decomposition temperature (°C)	314	262	153	135	175

The combustion method has been successfully used in the preparation of a large number of the ceramic oxide materials for a variety of applications which illustrated in Table 2. For example During the short span (> 15 years), many from the author's laboratory were becoming interested and attracted for producing fine grain size, crystalline and homogeneous ceramics at relatively low temperature and with reduced processing time. For example, Hwang, et al. [48] has investigated decomposition of the five fuels by acid or carbohydrazide. Some properties of five

fuels they select are shown in Table 1. The results of the thermal analysis show that there were different weight losses of organic fuels as presented in Figure 8. When using carbohydrazide as organic fuel, indicating that the chemical reaction took place very rapidly. But remaining weight is 22% of its original weight. While using glycine and alanine as organic fuels, the thermogravimetric of both demonstrated similar results. Their reactions are very fast and remaining weight lower than 10%. When using urea and citric acid as organic fuels, the chemical reaction was not rigorous when compared with glycine and alanine. Moreover, the crystal structure and microstructure of Ni-Zn ferrites prepared by combustion technique with various organic fuels was studies also. They result show that the pure phase of Ni-Zn was obtained while using glycine, alanine and corbohydrazide. While using urea and citric as organic fuels, the impurities phase was obtained existed in the diffraction pattern, as seen in Figure 9. The nanocrystalline sizes are ranging between 20.2 and 43.7 nm, as seen in Table 2. The results indicated that the ceramic synthesized by the combustion technique produced nanocrystalline sizes.

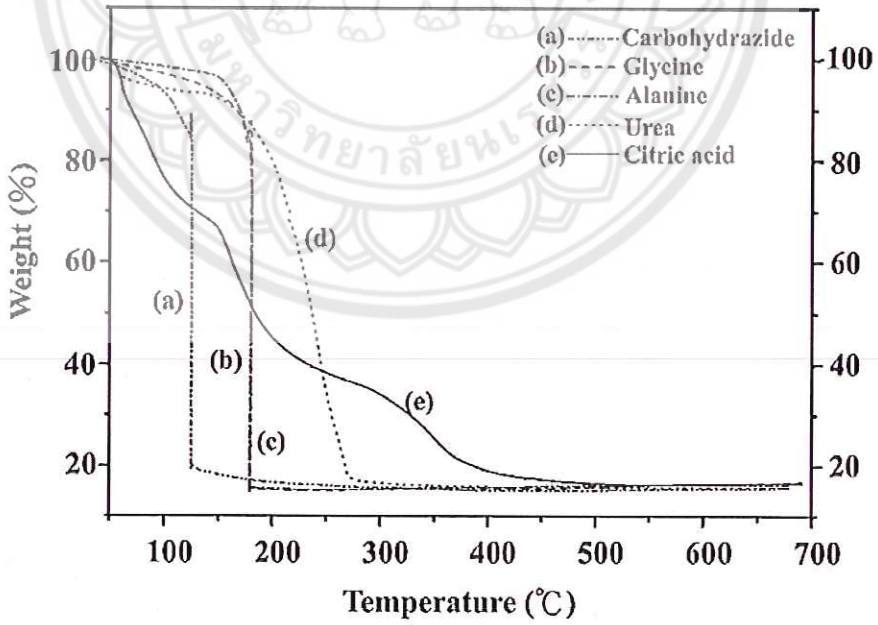

Figure 8 Thermogravimetric of various fuels [48]

Table 2 Oxide materials prepared by solution combustion method with the fuels

Material	Fuel	Particle size	Application
Al_2O_3	U	4 μm	Abrasive
Al_2O_3-ZrO_2	U	20-45 nm	Cutting tool
MAl_2O_4 (M=Mn and Zn)	AM+U/CH/ODH/GLY	15-28 nm	Catalytic support
$MgAl_2O_4$	U	13-20 nm	Structure material
CeO_2-ZrO_2	ODH	18 nm	Oxygen storage capacitor
	GLY	100 μm	Oxygen storage capacitor
$BaTiO_3$	GLY/CA	18-25 nm	Dielectric material
$Pb(Zr,Ti)O_3$	CA	~60 nm	Piezoelectric material
ZrO_2	GLY	23 nm	Oxygen sensor
$LiMn_2O_4$	PAA	30-60 nm	Lithium battery
$In_xGa_{1-x}O_3$	HY	54-160 nm	Optical coating for sensors
TiO_2	ODH	20 nm	Catalyst
	GLY	8-12 nm	Carcinogenic hexavalent chromium reduction
$LaBO_3$	U	55-75 nm (FESEM)	Decomposition of N_2O to N_2 and O_2
WO_3	GLY/U/thiourea	12-59 nm	Removal of organic dye from water
MgO	GLY	12-23 nm	Fluoride removal from drinking water

Note: U urea, AM metal acetate, CH carbohydrazides, ODH oxalidihidrazida, GLY glycine, CA citric acid, PAA poly acrylic acid, HY hydrazine. [49, 50, 51]

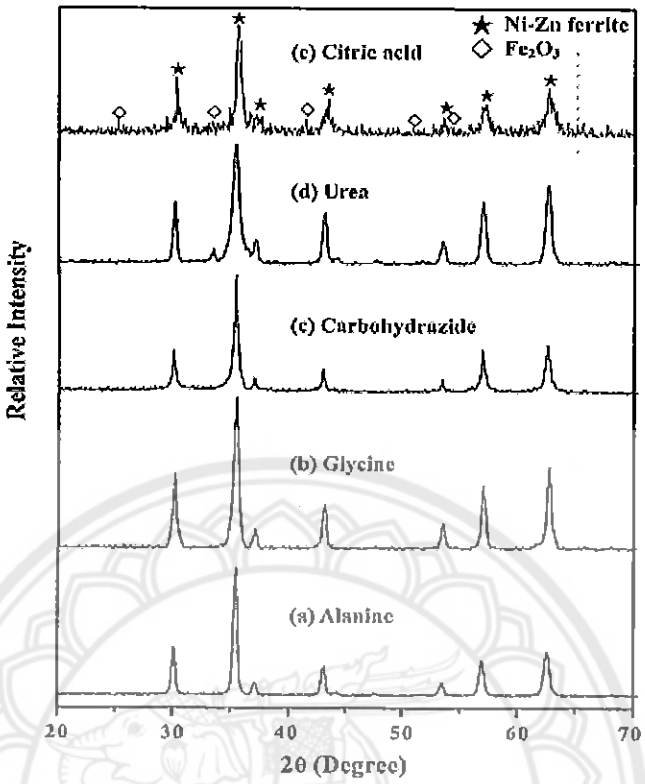

Figure 9 XRD patterns of the Ni-Zn ferrites with various organic fuels: (a) alanine (b) glycine (c) carbohydrazide (d) urea and (e) citric acid [48]

Wu, et al. [52] studied the effect of using various fuels on the structure and magnetic properties of SiO_2-doped Ni-Zn ferrite composite prepared by sol-gel combustion method. The result shows that the fuel type dramatically influenced the phase formation and electromagnetic properties of final products. The particle size for preparing its powders decreased in order: glycine route > hydrazine route > citric acid route, which are 34, 22 and 18 nm, respectively. Thus, citric acid was an effective chelating agent in producing fine ferrite powder. However, the glycine route was an effective fuel to possess the best magnetic properties with high saturation magnetization and low value of coercively.

Table 3 Effect of various fuels of the Ni-Zn ferrites prepared by the combustion technique [48]

Fuel	[a]T_m (°C)	Amount of gas produced (mole)	Crystallite size[b] (nm)	Surface area (m^2/g)	Carbon content (wt.%)	Ni^{2+} :Zn^{2+} : Fe^{3+}	[c]M_s (Am^2/kg)
Alanine	1245	20.7	38.6	24.7	1.64	0.500:0.467: 1.920	60.8
Glycine	1150	26.2	32.7	31/2	1.53	0.500:0.471: 1.922	62.4
Carbohydrazide	1380	24.0	43.7	20.6	1.87	0.500:0.462: 1.917	58.5
Urea	785	30.7	20.2	48.5	3.82	0.500:0.483: 1.936	57.2
Citric acid	725	26.2	22.7	44.1	5.75	0.500:0.490: 1.947	55.8

Note: [a]T_m the maximum combustion temperature, measured by Pt-Pt-Rh thermocouple.

[b]Crystalline size of the as-synthesized Ni-Zn ferrite powders calculated from the line broadening of the (311) XRD peak by Sherrer formula.

[c]M_s the saturation magnetization of the sintered Ni-Zn ferrite samples (950 °C/2h).

Lead free piezoelectric ceramics

Many of the piezoelectric materials used today are lead-based. The PZT family mentioned initially is the most common one. This is the binary solid solution of $PbZrO_3$ an antiferroelectric (orthorhombic structure) and $PbTiO_3$ a ferroelectric structure (tetragonal perovskite structure). PZT has the perovskite structure with the Ti^{+4} and Zr^{+4} ions at B site at random. The phase diagram shows that at high temperature PZT has the cubic perovskite structure which is paraelectric and on cooling below the curie point the structure under goes a phase change from the ferroelectric tetragonal phase to rhombohedral phase. PZT dominates the field of

piezoelectrics because of its strong piezoelectric effect, especially at the compositions near the morphotropic phase boundary $Pb(Zr_{0.52}Ti_{0.48})O_3$, where two ferroelectric phases tetragonal and rhombohedral coexist at the room temperature. The morphotropic phase boundary of PZT is almost vertical in the phase diagram, as shown in Figure 10 which maintains the excellent piezoelectric properties across a wide temperature range [29].

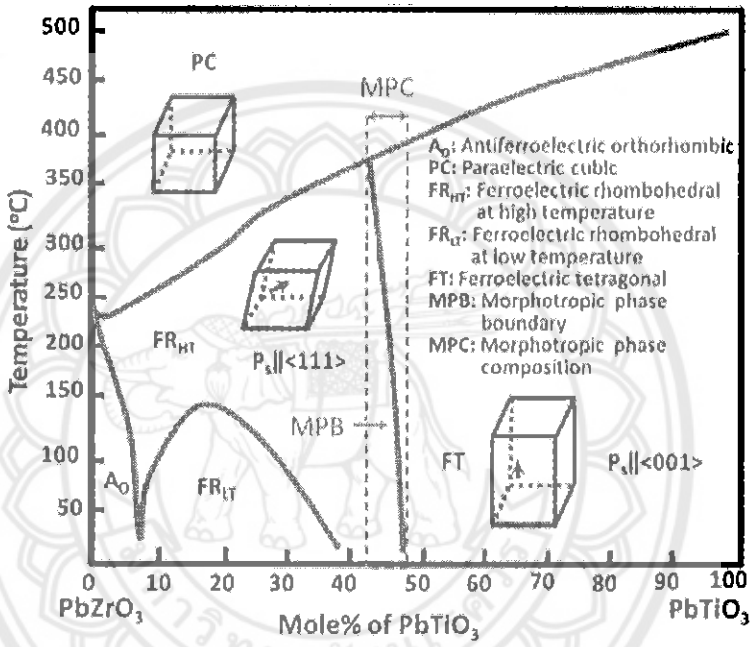

Figure 10 The phase diagram of PZT [29]

Some newer generations of lead-based piezoelectrics that exhibit exceptional piezoelectric properties have also been created by combining $PbTiO_3$(PT) with some lead-based ferroelectrics such as $Pb(Zn_{1/3}Nb_{2/3})O_3$ (PZN) and $Pb(Mg_{1/3}Nb_{2/3})O_3$ (PMN) to form solid solutions. Also, these materials show very high dielectric constants at room temperature owing to the broadening of the permittivity peak around the Curie temperature. PZT ceramics with MPB composition can also be doped with different ions and form "hard and soft" PZT is depending upon the requirements for certain applications [29].

The essential deficiency of Pb-based (PT, PZT and PMN) concerns its lead content. The amount of Pb in the usual Pb-based ceramics is more than 50 wt%, and once the Pb comes into the human body, it collects in various organs, leading potentially to serious effects to foetus, infertility, cancer and so forth. Note that not only the Pb in Pb-based compounds such as PT, PZT and PMN but also the PbO using as a raw material are known to dissolve when it is exposed to an aqueous environment However, high volatilization of PbO and its toxicity can pollute the environment and damage to human health, and then engender a terrible problem of environment pollution. However, these ceramics are toxic in the environment and damage to human health. The best way of prevention is to avoid the contact with leaded materials. Therefore, it is necessary in the search for lead-free piezoelectric materials to replace PZT ceramics.

Therefore, enormous efforts have been considerate in last decade for the development of competitive lead free counterparts, for example (K, Na)NbO_3 (KNN) and $BaZrO_3$ (BZ) based perovskite.

Potassium sodium niobate

Potassium sodium niobate (KNN) is considered as promising lead-free materials alternative to PZT a good candidate to replace PZT family. This system has an advantage of high Curie temperature (T_c~420 °C) suitable for wide temperature range of piezoelectric application. However, pure KNN solid solution exhibits relatively a low piezoelectric coefficient (d_{33}~80 pC/N) and poor remnant polarization (P_r~11 μC/cm^2). Moreover, pure KNN ceramics are very difficult to obtain at high density by traditional sintering processes because of the volatility of K^+ and Na^+ and the low phase stability at high sintering temperatures [65]. In order to improve the densification and the electrical properties of KNN ceramics, binary and ternary systems have been investigated by adding other elements.

Zuo, et al. synthesized the highly dense (1-x)($Na_{0.5}K_{0.5}$)NbO_3-x($Bi_{0.5}Na_{0.5}$)TiO_3 abbreviated KNN-BNT (x=0.005, 0.01, 0.02, 0.03, 0.05, 0.09, 0.15, 0.2, 0.8 and 1.0) solid solution ceramics. The KNN-BNT have been prepared consisted of the calcined powder and sintered ceramic at 900 °C for 5 h and 1090 °C for 2 h, respectively. The

SEM morphology of KNN-BNT ceramics was shown in Figure 11. The grain size changes from 3 to 4 μm for 0.99KNN-0.01BNT to ~0.6 μm for 0.95KNN-0.05BNT.

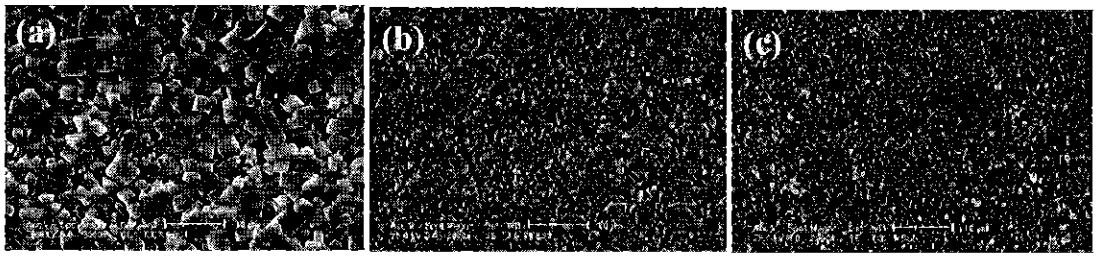

Figure 11 SEM micrographs of (1−*x*)KNN-*x*BNT ceramics sintered at 1090 °C with *x* equal to (a) 0.01, (b) 0.03 and (c) 0.05 [55]

The x-ray diffraction patterns of KNN-BNT ceramics were shown in Figure 12. All composition show pure perovskite structure. KNN was changed by adding a small amount of BNT. (1−*x*)KNN-*x*BNT ceramics at room temperature had orthorhombic structures similar to pure KNN, when $x \leq 0.02$. It becomes tetragonal when more BNT was added. However, the tetragonal symmetry remains in a limited composition range within which the tetragonality decreases with increasing the BNT content. The cubic structure starts to appear when x is greater than 0.09 until x=0.20 approximately when x continues to increase, NKN-BNT solid solutions exhibit rhombohedral structures until pure BNT composition which was known to be rhombohedral symmetry at room temperature.

(1−*x*)KNN-*x*BNT ceramics were investigated with their phase transition behavior and electrical characterization. A continuous phase transition was identified by adding a certain amount of BNT into KNN compositions, bringing about a MPB existing at 2–3 mol % BNT. Enhanced piezoelectric and electromechanical properties d_{33} =195 pC/N and k_p=43% (Figure 13) were obtained in the composition near the MPB. These compositions also have a comparable Curie temperature of 375 °C to that of PZT ceramics. These properties indicated that this system may be an attractive lead-free material for piezoelectric applications.

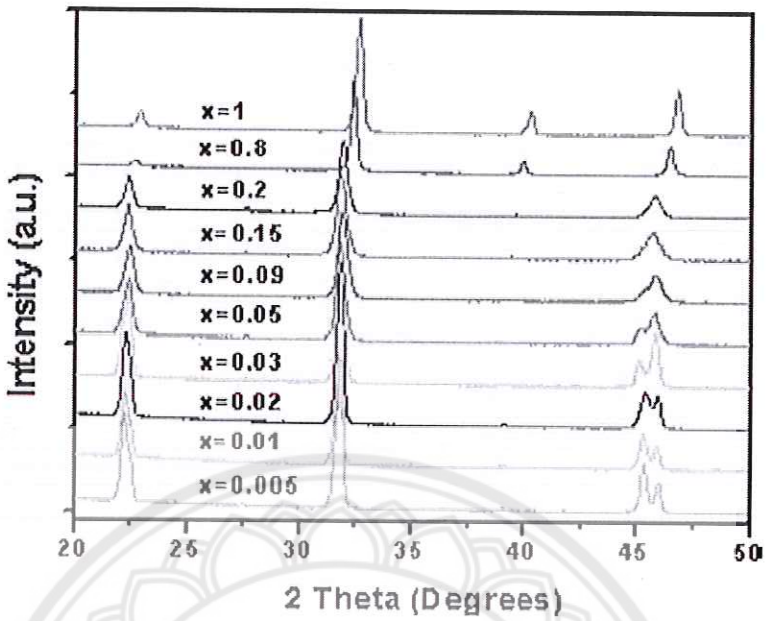

Figure 12 XRD patterns of (1-x)KNN-xBNT ceramics with x, as indicated [55]

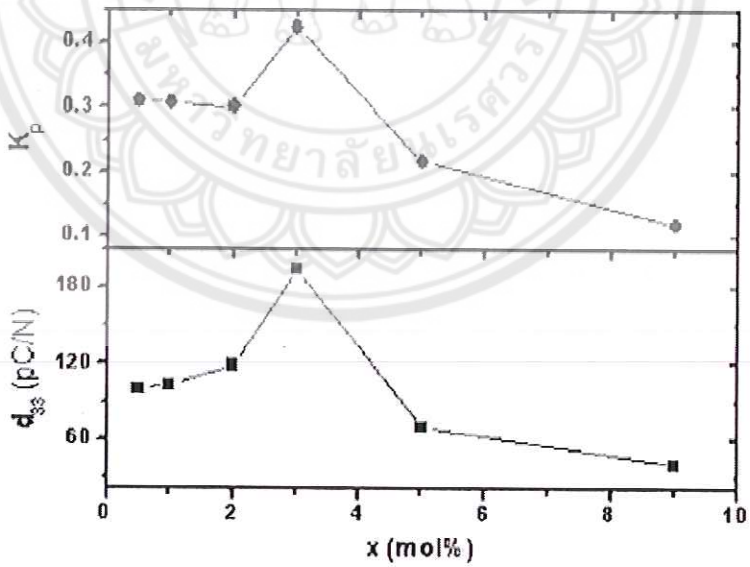

Figure 13 Piezoelectric constants and electromechanical coupling factors of (1-x)KNN-xBNT ceramics as function of the BNT content x [55]

Saito, et al. [56] presumed MPB compositions in the binary KNN- LiTaO3 (LT) system or ternary KNN-LT-LiSbO3 (LS) as shown in Figure 14. They found that the texture ceramic of the $(K_{0.44}Na_{0.52}Li_{0.04})(Nb_{0.84}Ta_{0.10}Sb_{0.06})O_3$ (L4FT) synthesized by the reactive template grain growth (RTGG) technique attains excellent piezoelectric constant d_{33} of ~400 pC/N.

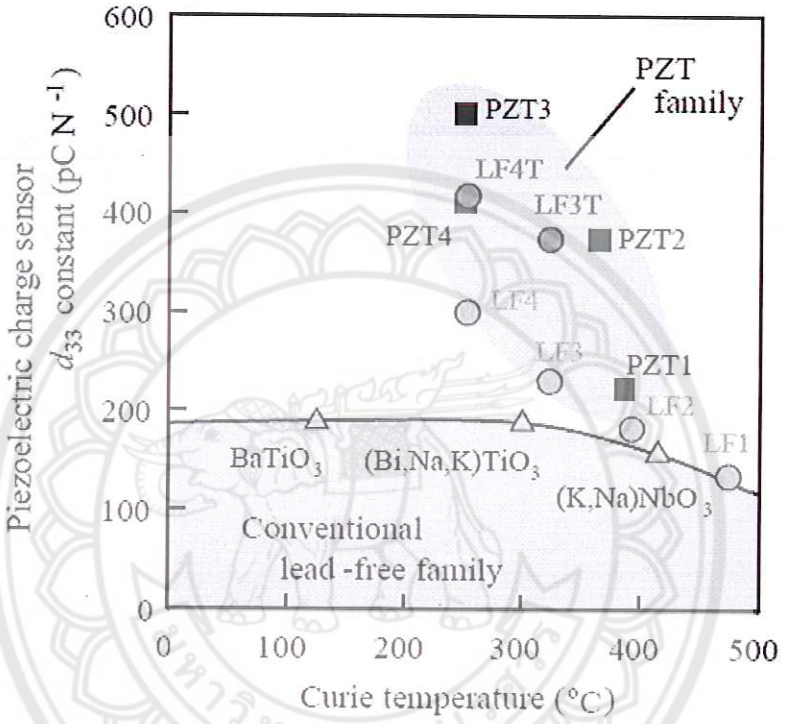

Figure 14 Piezoelectric sensor performances for the lead-free piezoelectric ceramics [56]

Jiang, et al. [57] reported the piezoelectric properties of (1-x) $(K_{0.44}Na_{0.52}Li_{0.04})(Nb_{0.84}Ta_{0.10}Sb_{0.06})O_3$-$xBiFeO_3$ (x=0, 0.002, 0.004, 0.006, 0.008 and 0.01) fabricated by conventional mixed-oxide technique using a calcination temperature of 880 °C for 6 h and a sintered temperature of 1135 °C for 3 h. The x-ray diffraction patterns of KNN-BNT ceramics were shown in Figure 15. All samples exhibited pure perovskite structure and no secondary phase could be found in all samples. The (1-x)(KNLNTS)-xBF ($x \leq 0.004$) ceramics are single perovskite phase with single orthorhombic crystal system. However, the symmetry changes rapidly with the addition of BF. The XRD patterns near at x = 0.004–0.006 show mixed phases.

When $x \geq 0.008$, it becomes a tetragonal perovskite structure. This result indicates that the transitional point for the structure change can be certified to be near $x = 0.004–0.006$. So a morphotropic phase boundary (MPB) between the orthorhombic and tetragonal ferroelectric phases of the (1-x)(KNLNTS)-xBF ceramics was identified in the composition range of 0.004–0.006.

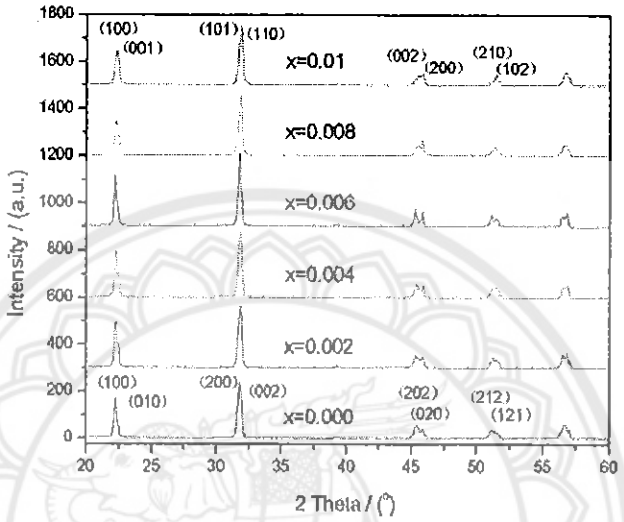

Figure 15 XRD patterns of BF doped KNN–LS–LT ceramics sintered [57]

Table 4 Density and electrical properties of KNLNTS–BF ceramics [57]

x	0	0.002	0.004	0.006	0.008	0.1
Bulk density (g/cm^3)	4.62	4.71	4.79	4.80	4.79	4.78
d_{33} (pC/N)	92	205	206	246	118	88
k_p	0.23	0.38	0.42	0.43	0.24	0.21
Q_m	94	138	130	94	130	140
Tan δ (%) (at 1 kHz)	4.62	2.88	2.86	1.96	3.05	3.24
ε_r (at 1 kHZ)	1096	1410	1494	1871	1611	1702
T_{o-t} (°C)	115	85	70	35	<25	<25
T_c (°C)	320	305	285	285	265	235

The piezoelectric properties of (1-x)(KNLNTS)-xBF ceramics were shown in Table 4. The best piezoelectric and electromechanical properties of d33 = 246 pC/N and kp = 43% appear at x = 0.006.

Hagh, et al. [58] synthesized $(K_{0.44}Na_{0.52}Li_{0.04})(Nb_{0.84}Ta_{0.10}Sb_{0.06})O_3$ system by two possible routes, namely perovskite and mixed oxides route and studied the effect of humidity and oxygen flow rate during sintering. In case of perovskite route using a sintering temperature of 1150 °C for 1 h. It was found that piezoelectric coefficient, remnant polarization and coercive field were 300 pC/N, 18 $\mu C/cm^2$ and 8.4 kV/cm, respectively. The samples were prepared under the following special conditions; (i) the raw materials were heat treated at 220 °C for 24 h, (ii) the powder process performed in glove box with Ar gas flowing and (iii) the samples were sintered in high O_2 atmosphere (360 cm^3/min). However, under ordinary conditions, KLNLTS ceramics exhibited a low electric properties as shown in Table 5.

Table 5 Processing property relationships for KNLNTS ceramics [58]

Property/processing step	Lab atmosphere perovskite rt.	High flow rate O_2 controlled atmosphere perovskite rt.	High flow rate O_2 mixed oxide w/high purity precursors
Relative permittivity, ε_{33}^T @ 1 kHz and RT	745	1590	~1650
Dielectric loss, tan δ - 1kHz @ RT (%)	3.5	1.7	~2
Piezoelectric charge coefficient, d_{33} (pC/N)	145	300	340-370
Planar coupling coefficient, k_p (%)	28	44	48
Remnant polarization, P_r ($\mu C/cm^2$) @ RT	14	22	28-30
Relative density (%)	92	96	>97
Coervice field, E_c (kV/cm)	13.3	8	8.8

The temperature dependence of the dielectric constant (ε_r) of KNLNTS ceramics measured at the frequency of 1 kHz. The temperature dependence of the dielectric constant of KNLNTS ceramics exhibited two peaks which corresponded to the orthorhombic-tetragonal phase transition (T_{o-t}) at 31 °C, and the tetragonal-cubic phase transition (T_c) at 264 °C (Figure 16). The dielectric constants (ε_r) at T_{o-t} and T_c were ~1175 and ~8000 , respectively.

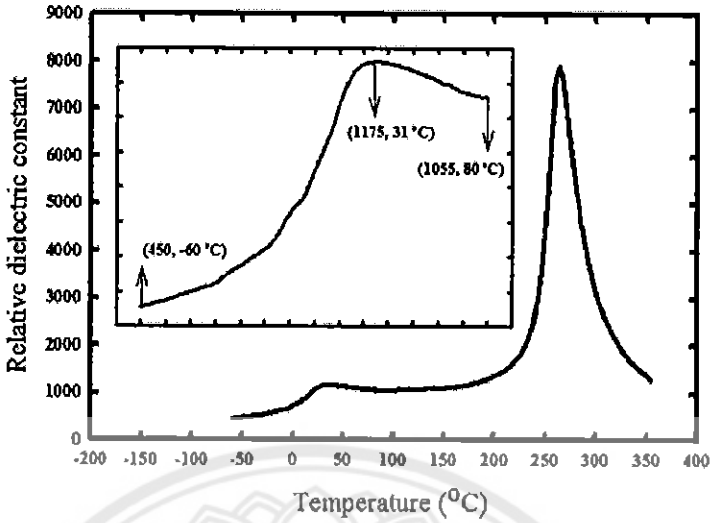

Figure 16 Variation of low-field 1kHz relative dielectric constant with temperature in $(K_{0.44}Na_{0.52}Li_{0.04})(Nb_{0.84}Ta_{0.1}Sb_{0.06})O_3$ [58]

Barium zirconate

Barium zirconate ($BaZrO_3$) is one of the perovskite material with an ideal cubic structure and has a high melting point of about 2,600 °C. Barium zirconate is a good candidate for many applications.

A.M. Azad and S. Subramaniam [59] synthesized pure cubic perovskite $BaZrO_3$ powder using the solid reaction method and a sintered temperature from 1200 to 1700 °C. The x-ray diffraction patterns of $BaZrO_3$ ceramics were shown in Figure 17. All samples exhibited pure perovskite structure and no secondary phase could be found in all samples. The crystallite size ranged between 0.36 and 0.44 μm. The microstructural development in samples soaked for 6 h at 1400 and 1500 °C was shown in Figure 18. The microstructure reveals better intergranular connectivity, systematic grain growth and steadily diminishing porosity. However, the bodies sintered in the range 1200-1400°C were quite fragile and had a rather low strength. The sintered pellets could easily be broken under slight pressure. With increase in sintering temperature (1500–1700°C), densification improved systematically with corresponding decrease in porosity (mainly open pores). The average size is less than 1 μm in all the cases. the compacts showed increase in strength, especially those sintered at 1600 and 1700 °C as shown in Figure 19.

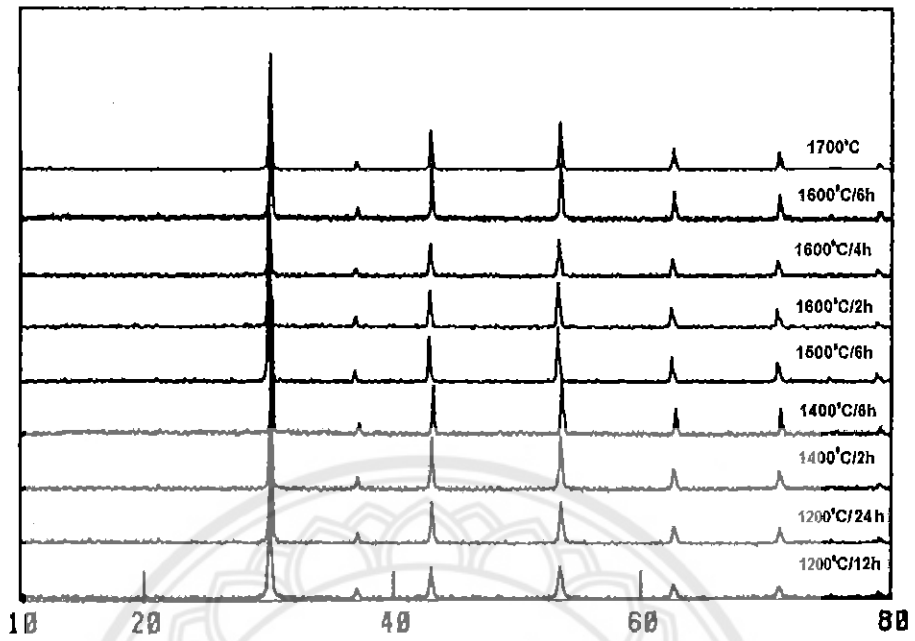

Figure 17 XRD patterns of $BaZrO_3$ sintered in the range 1200–1700 °C [59]

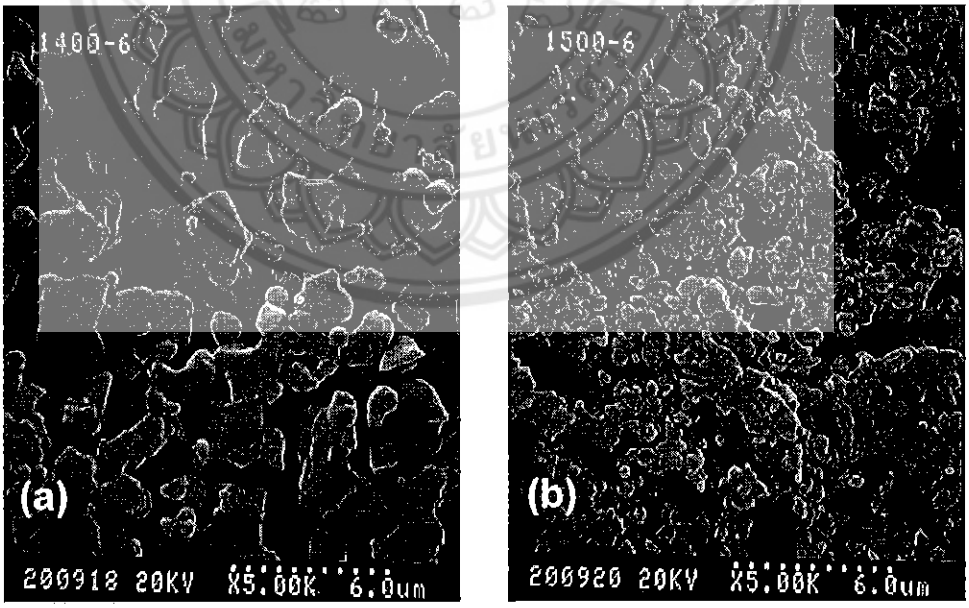

Figure 18 Microstructural development (clockwise) in $BaZrO_3$ soaked for 6 h at (a) 1400 and (b)1500 °C [59]

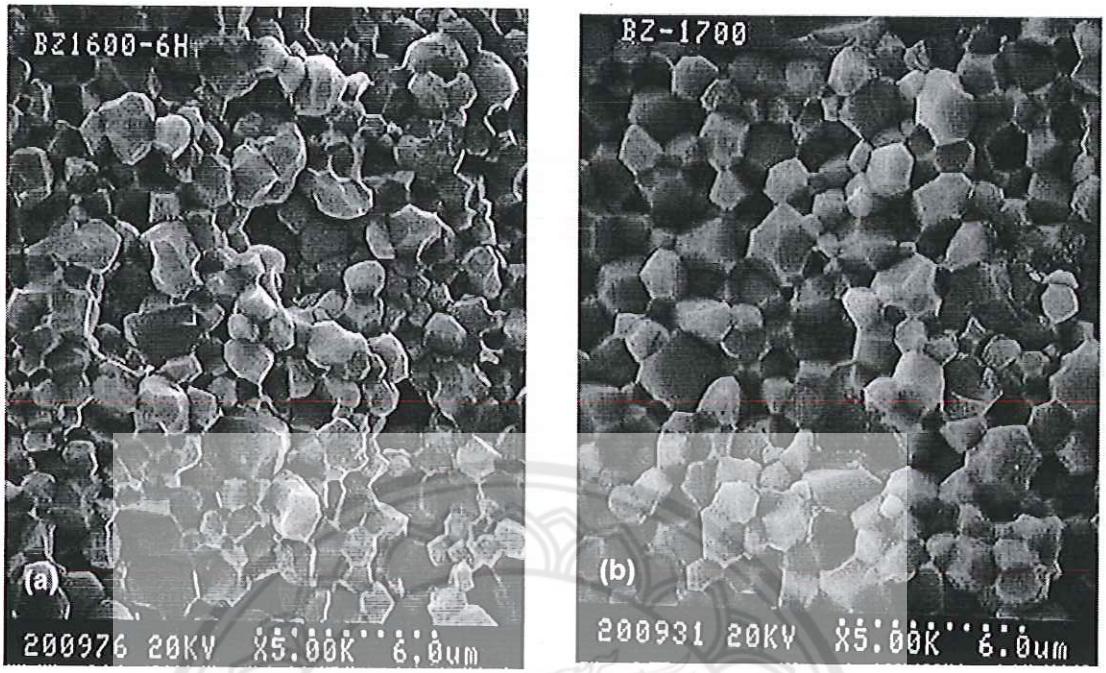

Figure 19 Enhanced densification and intergranular connectivity in $BaZrO_3$ sintered at (a) 1600°C and (b) 1600°C for 6h and 1700 °C no soak [59]

Sin, et al. [60] reported a value of 95% of theoretical density of $BaZrO_3$ ceramics. They synthesized nano $BaZrO_3$ powders by the polyacrylamide method. The sintered ceramics were obtained using a heat treatment of 1,500 °C for 10 h. Ganguli, et al. [61] synthesized Nano $BaZrO_3$, powders (25-30 nm) and low firing temperatures (calcined at 800 °C, sintered at 1,000 °C) were obtained using microemulsion route. Guillaume et al. [62] successfully prepared 99% of theoretical density of $BaZrO_3$ ceramics by control the calcined powder size distribution. The mean particles size of 600 nm was sintered at 1,650 °C for 2 h.

A.M. Azad and S. Subramaniam [63] attempted to improve the density and dielectric properties by adding 5 mol% Sn in $BaZrO_3$. The attempt to improve the density was not successful but with a dielectric loss of the $Ba(Zr_{0.95}Sn_{0.05})$ ceramics exhibited a very small value and were stable in a wide frequency range ($1\text{-}10^6$ Hz).

Li, et al. [64] studied the system of $(Ba_{1-x}Ca_x)(Ti_{0.94}Sn_{0.06})O_3$ (BCST) (x=0.01-0.04) ceramics by the solid state reaction technique. The microstructure of BCST ceramics at x = 0.01 is inhomogeneous and some pores exist in the grain boundary. For the samples at x = 0.02 and 0.03, the microstructure is homogeneous and no pore exists in the grain boundary, while the grain size is about 10 μm. For the sample at x = 0.04, the microstructure is inhomogeneous and the grain size becomes small (5 μm) as shown in Figure 20. The relative density are 96%, 98%, 99% and 97% for the BCST.

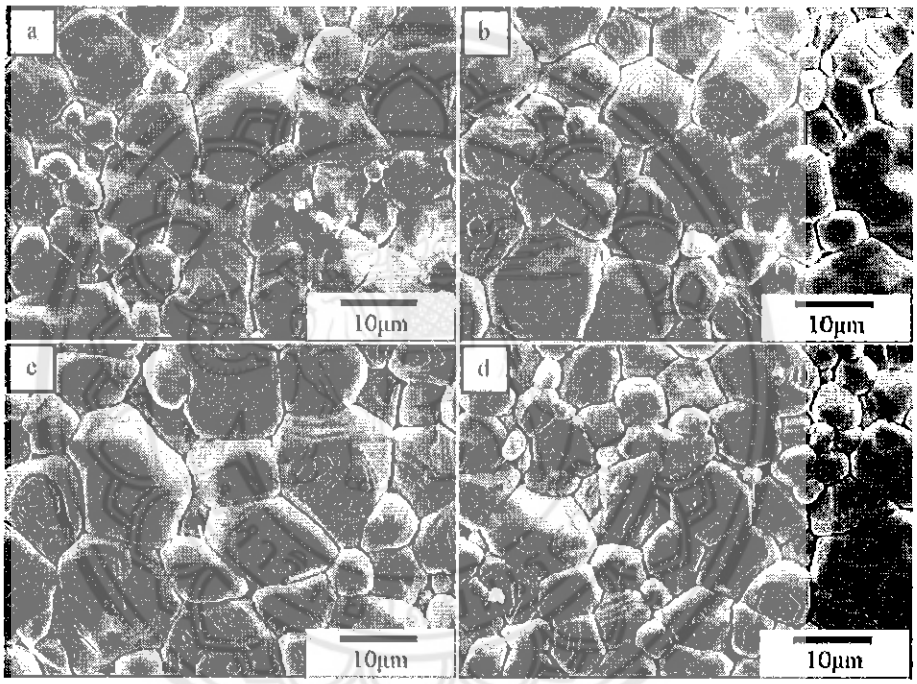

Figure 20 SEM micrographs of the $(Ba_{1-x}Ca_x)(Ti_{0.94}Sn_{0.06})O_3$ ceramics (a) x = 0.01, (b) x = 0.02, (c) x = 0.03 and (d) x = 0.04 [64]

The substitution of Ca promoted the microstructure of $Ba(Ti_{0.94}Sn_{0.06})O_3$, which presented a clear grain boundary and a uniformly distributed grain size. It also resulted in increased density and better electrical properties. $(Ba_{0.97}Ca_{0.03})(Ti_{0.94}Sn_{0.06})$ which exhibited excellent piezoelectric properties (d_{33}=440 pC/N, kp=45%), a high dielectric constant (ε_r= 6,900) and a low dielectric loss (tan δ=0.015).

CHAPTER III

MATERIALS AND METHOD

In this chapter explains the fabrication and characterization of (1-x)BNKLLT-xNKLNST with $0 \leq x \leq 0.10$ solid solution. All powders fabrications were prepared by the solid state combustion method. The characterizations of these powders were observed using XRD, and SEM. The ceramics were characterized to find out their properties such as physical properties, phase formation, microstructure and electrical properties. The details are presented in the following sections.

Preparation of (1-x)BNKLLT-xNKLNST ceramics

(1−x)BNKLLT–xNKLNST lead-free piezoelectric ceramics with an x concentration between 0 and 0.10 were synthesized using the solid state combustion method [19-23] and the fuel used was glycine (>98.5%, Ajax, NZ). In this process, highly pure reagents were used as raw materials: Bi_2O_3 (>99%, Qrëc, NZ), $NaNO_3$ (>99%, Ajax, NZ), $KHCO_3$ (>99%, Ajax, NZ), Li_2CO_3 (>99%, Merck, DE), TiO_2 (>99%, Ajax, NZ), La_2O_3 (>99%, Aldrich, CN), Nb_2O_5 (>99%, Ajax, NZ), Sb_2O_3 (>99% Ajax, NZ) and Ta_2O_5 (>99%, Cerao, US). All raw materials were weighed using the following stoichiometric ratio, $Bi_{0.5}(Na_{0.68}K_{0.22}Li_{0.1})_{0.5}TiO_3$+0.1wt% of La_2O_3 (BNKLLT) [4] and $(K_{0.44}Na_{0.52}Li_{0.04})(Nb_{0.84}Ta_{0.10}Sb_{0.06})O_3$ (KNLNTS) [24]. They were then ball milled in ethanol for 24 h and then dried on a hot-plate at 80°C. The dried BNKLLT and KNLNTS powders were mixed with glycine in a ratio of 1:0.56, and then the mixed powders were calcined at 750°C and 650°C for 2 h, respectively [4, 24]. Afterwards, the calcined powders of BNKLLT and KNLNTS were mixed with different compositions and were again ball milled with 3 wt% aqueous PVA in ethanol for 24 h. After that, the mixed calcined powders were pressed into pellet discs with ~1.5 cm diameter and ~1.2–1.5 mm thickness. The green pellets were sintered at 1100°C for all compositions using a dwell time of 2 h [4] in air with a heating rate of 5°C/min and allowed to cool down naturally. The sintered samples

were coated with silver paste (Heraeus, D11402) on both sides and were annealed at 500°C for 30 min in order to characterize their electrical properties. For piezoelectric testing, the samples were poled in a silicon oil bath under a 4 kV/mm dc field at 70°C for 30 min. The electric field was then decreased to zero kV/mm and the samples were cooled down to room temperature.

Sample Characterization

The following section addresses the main characterization techniques used to investigate the phase formation, morphology, particle size, microstructure, physical properties and dielectric property of the samples in this study. They are described below.

X-ray diffraction (XRD) Technique

The X-ray diffraction (XRD) was used to identify the optimum firing temperatures, for phase identification, quantitative analysis of the mixtures of phases, and also to determine the crystal structure of the samples at room temperature, in both powder and ceramic forms. The X-ray diffractometer (Philips model X'Pert Pro) with Cu Kα radiation at 20 kV was employed as shown in Figure 21. Each sample was scanned for a 2θ range from 10°-60°. Lattice parameters of sample were determined from X-ray powder diffraction database from ICDD. The crystallite size of the calcined powder and ceramics grain size were also determined using the XRD line broadening as derived by Scherer equation [53];

$$B_{crystallites} = \frac{k\lambda}{L\cos\theta} \tag{5}$$

Where B is a broadening of the diffraction line measured at half its maximum intensity, L is the average crystallite size and k is a constant

The relative amounts of the perovskite and pyrochlore phases were calculated from the intensities of major X-ray reflections of the pyrochlore phase as perovskite phase using the equation proposed by Swart and Shrout [54];

$$\%Perovskite = \frac{I_{perovskite}}{I_{perovskite} + I_{pyrochlor}} \times 100 \quad (6)$$

Where $I_{perovskite}$ refers to the intensity of the peak of the perovskite phase and $I_{pyrochlore}$ refers to the intensity of the highest peak of pyrochlore phase.

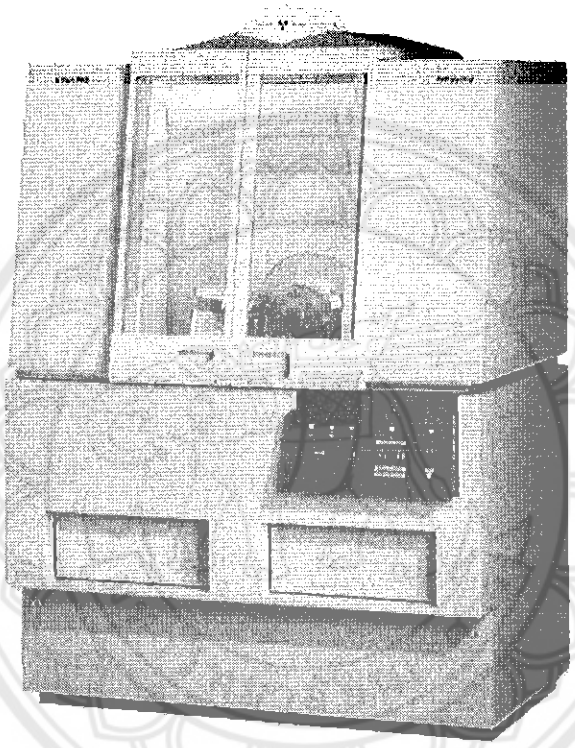

Figure 21 X-ray diffractometer [66]

Scanning electron microscopy (SEM)

Microstructural characterization of sample surface using scanning electron microscopy (SEM) (Figure 22) was performed to determine the grain size and the presence of porosity. Average grain size of the sintered ceramics were estimated by using a linear intercepting method, where random linear lines (L) were drawn on each SEM micrograph and the number of the intercepts which the grain boundary makes with the line (N). The average grain size (D) was determined from measurements along random lines using the equation [67];

$$D = \frac{L}{N} \quad (7)$$

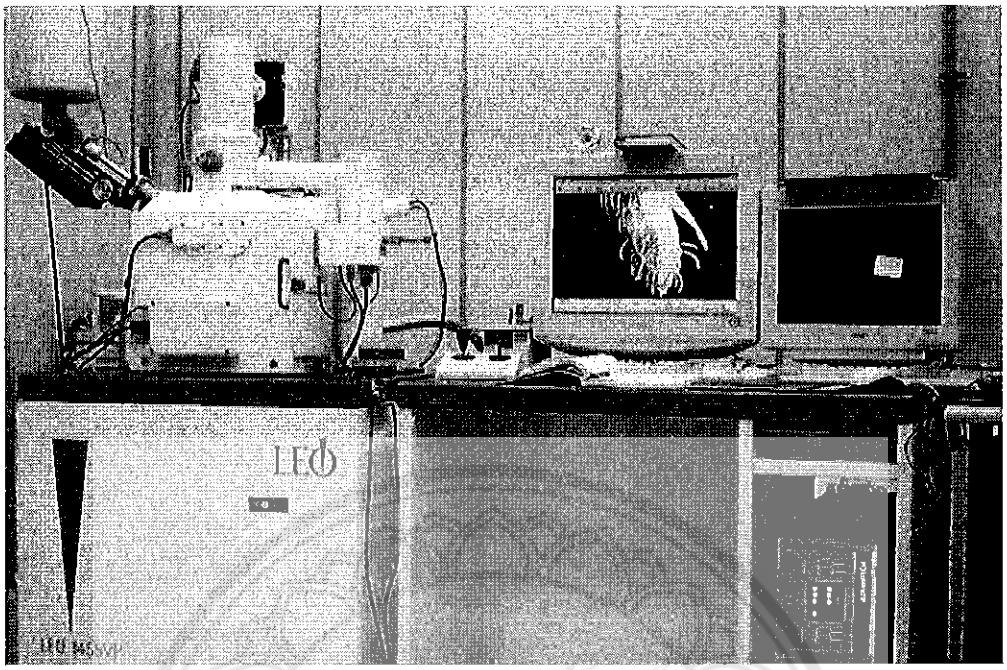

Figure 22 Scanning electron microscopy [66]

Transmission electron microscopy (TEM)

Transmission electron microscopy (TEM) (Figure 23) was employed to investigate the morphology of the powders. Samples for TEM were prepared by grinding, dispersing them in isopropyl alcohol and then depositing the sample by pipette onto 3 mm holey copper grids for observation by TEM (FEI, Technai G2).

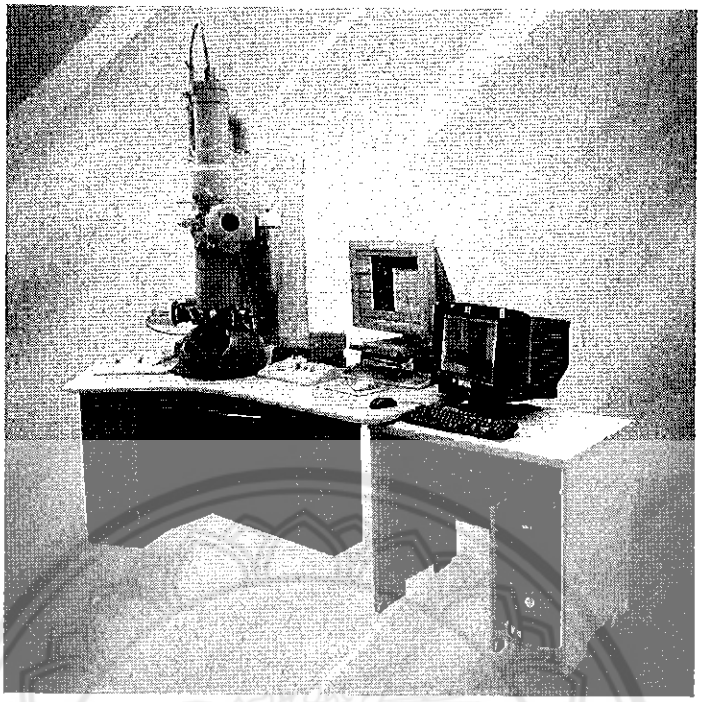

Figure 23 Transmission electron microscopy [66]

Densification analysis

The method of measuring the density of a piece of ceramics material usually described in standards is based on the Archimedes principle. This principle stated the weight of an object in a fluid equals it's by weight minus the buoyant force (or the weight of the fluid displaced). However, it is usual to measure open porosity levels at the same time by ensuring that during immersion liquid can penetrate all parts of the specimen through the open porosity. Typical procedures are;

1. Dry specimen(s) in air at 110 °C, store in a desiccator, weigh when cold (mass W_1)

2. Boil in distilled water for a period, typically 3 hours and leave it for 1 night

3. Weigh immersed in water (W_2) and then weight during immersion liquid can penetrate all parts of the specimen through the open porosity (W_3).

4. Calculate follow this equation:

$$\rho_c = \frac{W_1 \rho_w}{W_3 - W_2} \quad (8)$$

where, ρ_w is the density of water at room temperature (g/cm^3) and is the density of sample at room temperature (g/cm^3); however the density of water is slightly temperature dependent

$$\rho_w = 1.0017 - 0.0002315T \quad (9)$$

Moreover, the fired shrinkage of all sintered ceramics were measured from the percentage diameter change with respect to the original diameter (l_0) before sintering;

$$Shrinkage(\%) = (\frac{l_1 - l_0}{l_0})x100 \quad (10)$$

where l_1 is diameter of pellet before sintering (mm),
l_0 is diameter of pellet after sintering (mm)

Dielectric measurement

The dielectric properties of the sintered ceramics were studied as functions of both temperature and frequency with an automated dielectric measurement system. The measurement system which measured the dielectric properties consisted of a LCR meter (Agilent 4263B). The dielectric properties were determined over a temperature range from room temperature to 200 °C with different frequencies (3 frequency of 1 kHz, 10 kHz and 100 kHz). The dielectric constant (ε_r) was calculated with the following equation,

$$\varepsilon_r = \frac{Cd}{\varepsilon_0 A} \quad (11)$$

where ε_0 is the permittivity of free space,
C is the capacitance,
D is the thickness of the sample,
A is the area of the sample.

P-E measurement

P-E measurement was made using high voltage amplifier (Trek), precision High Voltage Interface (HVI, Radiant Technologies), precision LC (Radiant Technologies) and computerized control and data acquisition. The sample is placed in a High Voltage Test Fixture chamber (HVTF) chamber in bottom half of the fixture. A copper electrode fixed in the bottom of the chamber contacts the electrode on the bottom of the sample. The bottom chamber is sealed so it may be filled with insulating oil to protect the sample from the arcing that may occur in open air. The system is an automated device intended for measuring the polarization of materials induced by a single triangle wave. It can prevent the excess voltage and current during a sample breakdown from exceeding the current canceling capability of the virtual ground circuitry on the tester input. During the measurement, an electric field of 30 kV/cm based on the coercive field was applied to a sample which immersed in a silicone oil to prevent the breakdown of the sample.

Piezoelectric properties measurement

The optimum poling conditions were determined by poling the KNLNTS ceramics with applying DC field of 3 kV/mm in a stirred oil bath at 80°C for a time period 30 minutes. The piezoelectric constant (d_{33}) was measured using a quasi-static piezoelectric d_{33} meter. The piezoelectric constant (d_{33}) measurements were made directly after poling and after 24 hours. Measurements were conducted at a drive frequency of 100 Hz.

CHAPTER IV

FABRICATION OF NEW LEAD-FREE (1-x)BNKLLT-xNKLNST CERAMICCS BY THE SOLID STATE COMBUSTION TECHNIQUE

X-ray diffraction patterns of (1-x)BNKLLT-xNKLNST ceramics at various compositions (x = 0, 0.02, 0.04, 0.06, 0.08 and 0.10) are represented in the Figure 24 (a). A structure of pure perovskite phase, without any detectable second phase, was observed. This indicates that the NKLNST was completely distributed into the BNKLLT lattice and a new homogenous solid solution was produced. In order to get insight into the phase formation of the effect of x content on structural (1-x)BNKLLT-xNKLNST ceramics, the expanded XRD patterns with 2θ around 40° and 46° are presented in Figure 24 (b) and (c). For the rhombohedral phase, the characterization exhibited the dual $(003)/(021)_R$ peaks at 2θ around 40° and a single $(202)_R$ peak at 2θ around 46° [4, 16]. The consideration for the tetragonal phase, it exhibited a single peak of $(111)_T$ and dual peaks of $(002)/(200)_T$ at 2θ around 40° and 46°, respectively [4, 16]. At the concentration of x = 0, a vague splitting of $(003)/(021)_R$ dual peaks (Figure 24 (b) I) was observed in the peak positioned at 40° and none symmetry of a single $(202)_R$ peak was observed at the peak positioned at 46° (Figure 24 (c) I) which assumed the coexistence between rhombohedral and tetragonal phases. This result was similar with BNKLLT ceramics synthesized by the combustion technique [4]. When the x concentration was increased from 0.02 to 0.06, the original doublet $(003)/(021)_R$ peaks position merged into a single peak of $(111)_T$ (Figure 24 (b) II-IV) while a skew left of $(202)_R$ peak continuously split into the dual $(002)/(200)_T$ peaks (Figure 24 (c)

II-IV), which assumed the tetragonality in these ceramics increased. When the x concentration was higher than 0.06, the peak position of (111) at 40° exhibited more symmetry (Figure 24 (b) V, VI) while the dual $(002)/(200)_T$ peaks at 46° began to fuse into single $(200)_C$ peak (Figure 24 (c) V, VI) which indicated that phase formation change to pseudo cubic phase.

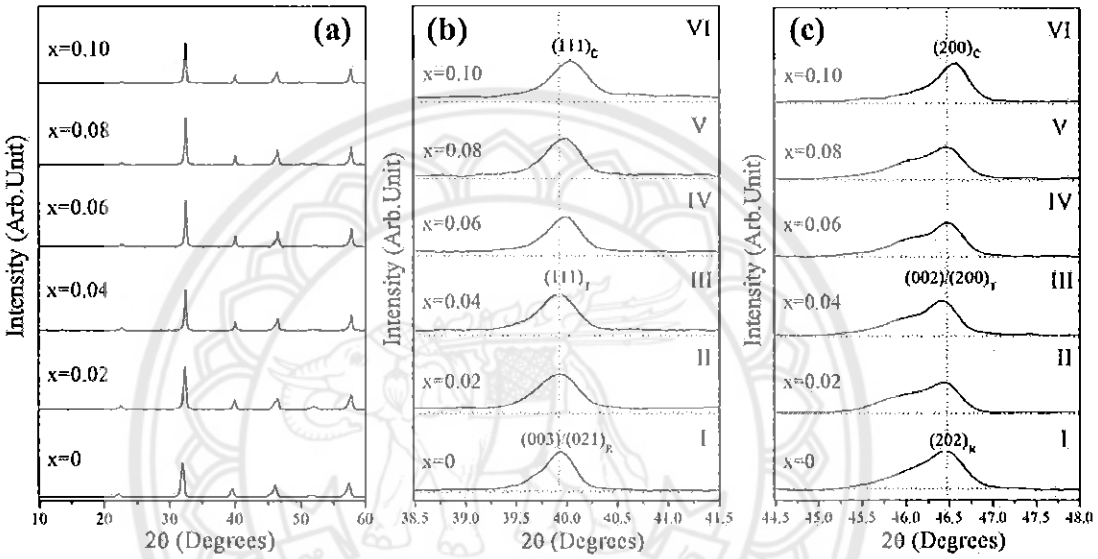

Figure 24. XRD patterns of the (1-x)BNKLLT-xNKLNST ceramics as a function of x concentration in 2θ range of (a) 10-60°, (b) 38.5-41.5° and (c) 44.5-48°.

Typical SEM morphology images of the polished and thermally etched surfaces of the (1-x)BNKLLT–xNKLNST ceramics with various x concentration are shown in Figure 25 (a)-(f). A polyhedral shape of the grain morphology was observed in all samples (Figure 25 (a)-(f)). At $0 \leq x \leq 0.02$ content, the border of polyhedral grain shape showed rounded corners (Figure 25 (a)-(b)). When x concentration increase of 0.04, the sharpness of the corners and grain boundaries were observed from the morphology images as shown in Figure 25 (c). When the x concentration was between 0.06 and 0.10, the rounded corners appeared at the boundary of the polyhedral grains

(Figure 25 (d)-(f)). Moreover, the grain size distribution of (1-x)BNKLLT-xNKLNST ceramics was narrower with increasing x concentration from 0 to 0.04 (Figure 25 (a)-(c)) and then exhibited a wider distribution with higher x concentration (Figure 25 (d)-(f)). The average grain size of (1−x)BNKLLT–xNKLNST samples with various x content was in the same range of 1.36-1.52 μm as listed Table 6. The density of the (1-x)BNKLLT-xNKLNST ceramics as a function of x concentration is reported in Table 6. The measured density value of these samples was about 5.59 to 5.78 g/cm^3 (Table 6). The relative theoretical density increased from 96.7 to 97.2% when the NKLNST concentration was increased up to 0.04 and then decreased in values as listed in Table 6. The density result of the (1-x)BNKLLT-xNKLNST samples corresponded with the microstructure result.

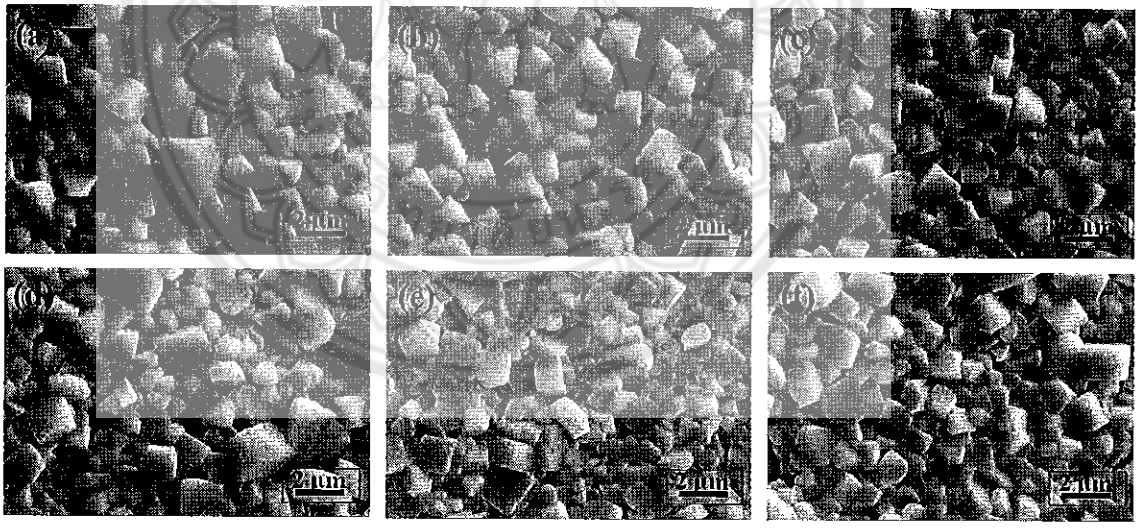

Figure 25 SEM surface microstructure of (1-x)BNKLLT-xNKNLST ceramics with different x concentration; (a) x = 0, (b) x = 0.02, (c) x = 0.04, (d) x = 0.06, (e) x = 0.08 and (f) x = 0.10.

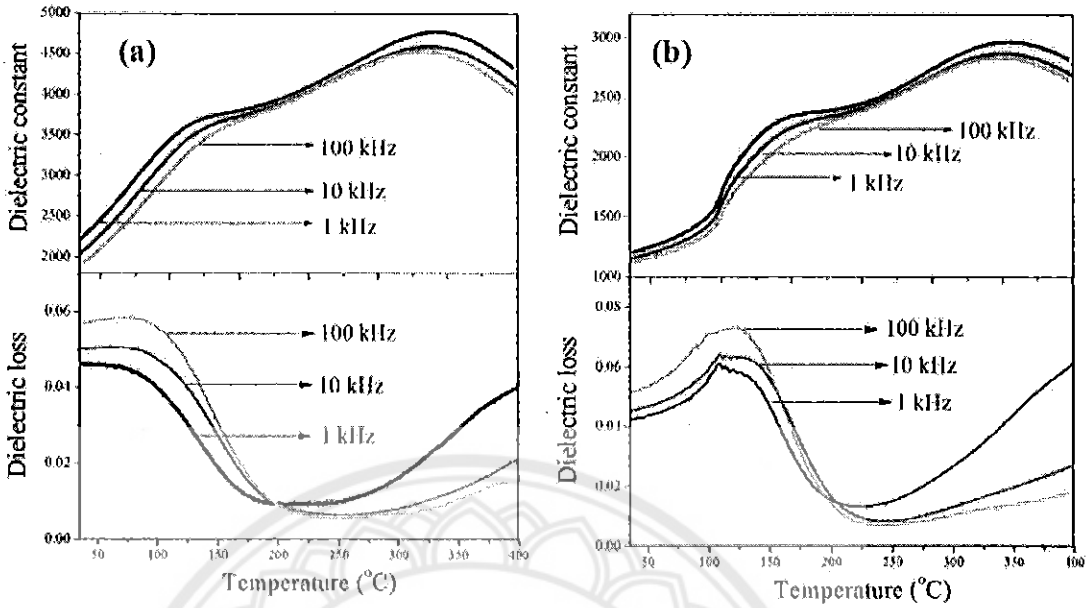

Figure 26 Temperature dependent of the relative permittivity of (1-x)BNKLLT–xNKLNST ceramics at x concentration of 0.04 measured at frequencies between 1 and100 kHz; (a) unpoled and (b) poled.

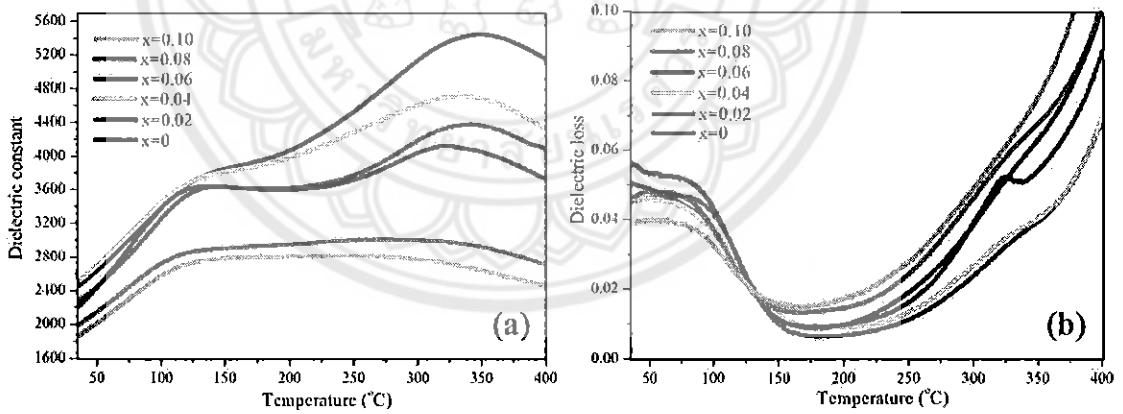

Figure 27 Temperature dependences of the relative permittivity at 1 kHz of the (1-x)BNKLLT-xNKLNST ceramics with function of x concertation (a) dielectric constant and (b) dielectric loss.

The plotted temperature dependence of the relative permittivity as a function of unpoled and poled (1-x)BNKLLT-xKNLNST ceramic at x concentration of 0.04 measured between 1 and 100 kHz is shown in Fig 3. For the unpoled sample (Figure 26(a)), the dielectric anomaly (ε) consisted of two broad dielectric curves, the first curve of a frequency dispersion occurring at a lower temperature (It will be assigned by a subscript "FA") and the second curve occurring at higher temperature (It will be assigned by a subscript "SA"). The curve of dielectric loss showed a broad peak shape at a lower temperature (tan δ_{FA}) and strong frequency dispersion. The temperature for tan δ_{FA} was less than that in the dielectric constant (ε_{FA}). At higher temperatures, the dielectric loss peak (tan δ_{SA}) presented a frequency dispersion and the magnitude of the peak value decreased with increasing frequency. These results were similar with the dielectric results of BNT- 6mol% BT, BNT-BKT modified with BZT and BNKLLT-4 wt% BCTZ in previous works, which were reported by C. Kornphom et al [5], W. Jo et al [26], and R. Dittmer et al [27], respectively. They indicated that the changing of dielectric curve be related with a thermal evolution of relaxation time distribution or correlation length distribution of the polar nanoregions (PNRs), which has nothing to do with any measurable phase transition [5, 26, 27]. The poled dielectric constant and loss of (1-x)BNKLLT-xNKLNST ceramics are presented in Figure 26(b). A discontinuous change in dielectric constant and loss was observed at ~110 °C, which corresponded to the temperature where the electric field induced ferroelectric order transform back to relaxer [26, 27].

The temperature dependence of the relative permittivity at 1 kHz of the (1-x)BNKLLT-xNKLNST ceramics as a function of x concentration between 0 and 0.10 is presented in Figure 27. It was observed that the dielectric response demonstrated

two anomaly peaks of ε_{FA} and ε_{SA} near 123-134°C (T_{FA}) and 323-338°C (T_{SA}), respectively. In samples with x concentration between 0-0.06, both T_{FA} and T_{SA} shift to a lower temperature with increasing x concentration (Table 6). It is generally accepted that the dielectric constant is related to domain alignment and structure. The reduction of T_{FA} and T_{SA} could be a consequence of ferroelectric order destabilization and the formation of a non-polar (NP) phase induced by the NKLNST addition [15, 16]. Moreover, an increment in the NKLNST concentration ($x \geq 0.08$) broadened the dielectric anomalies at T_{FA} and T_{SA}, which was similar to that proposed for the BNT-KNN ceramics [15]. The values of the dielectric constant at room temperature (ε_r) and maximum dielectric constant (ε_{SA}) of these samples were observed to decrease significantly (Table 6), this was similar to previous work of (1-x)BNT-xNKLNST ceramics [16]. The reduced ε_r and ε_{SA} was caused by the NKLNST introducing more ions into A and B-sites of BNKLLT perovskite structure leading to cation disorder and diffuseness [15, 16]. The dielectric loss (*tanδ*) at room temperature (T_r) and at T_{SA} of (1-x)BNKLLT-xNKLNST are listed in Table 6.

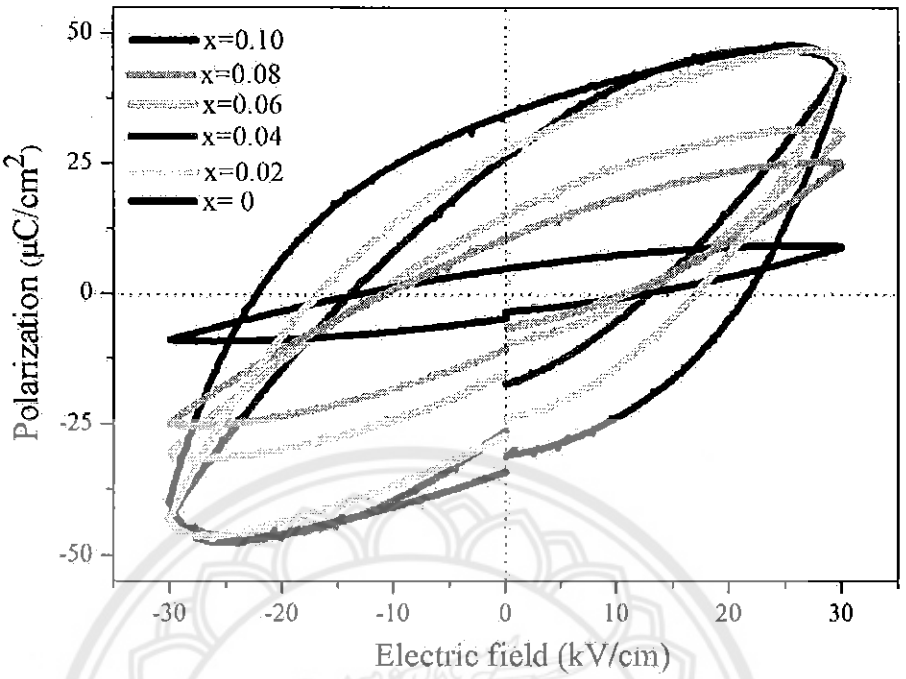

Figure 28. P–E loops of (1-x)BNKLLT–xNKLNST ceramics at different x content, measured at 30 kV/cm and room temperature.

Figure 28 shows the polarization hysteresis of (1-x)BNKLLT-xNKLNST ceramics with a distinct x content, the measurement was taken under an electric field of 30 kV/cm. From the image it can be seen that all samples exhibited unsaturated hysteresis loop, which was similar to results found in previous research [15, 16]. The measurements showed a large remnant polarization (P_r) and large coercive field (E_c) of the pure BNKLLT ceramic 35.8 μC/cm^2 and 22.42 kV/cm, respectively (Table 6). The slender P-E loops were observed and the P_r and E_c were greatly reduced when x content increased ≥ 0.02 (Table 6). This result indicates that the concentration of NKLNST compound inhibits a field-induced FE order and is similar with the previous observation in the BNT-KNN system [15]. Apparently, the increase of NKLNST content ≥0.06, both Pr and Ec steeply decreased and showed the thin loops, indicating

that the concentration of NKLNST compound disrupted the long-range ferroelectric (FE) order of the BNKLLT ceramics [15, 16].

The piezoelectric properties (d_{33}) at room temperature of (1-x)BNKLLT-xNKLNST system with different x content is listed in Table 6. The d_{33} values increased from 210 pC/N to 266 pC/N when x content increased from 0 to 0.04. Then, the d_{33} values reduced in turn with a further increase of NKLNST contents >0.04. The x concentration of 0.04 achieved a maximal d_{33} value of 266 pC/N. This was much higher than both the BNKLLT ceramic and the binary system of BNT-NKLNST, for example, when BNKLLT was produced from the solid state reaction method and solid state combustion technique, d_{33} was about ~192 and ~210 pC/N [4, 28]. The d_{33} value was about ~158 pC/N for binary BNT-NKLNST ceramics [16]. It is well known that a high piezoelectric constant (d_{33}) can be obtained from a coexistence phase because the direction of polarization is easily rotated by external stress or the electric field resulting from the instability of the polarization state [5, 15, 16]. Thus, a (1-x)BNKLLT-xNKLNST ceramics with x concentration of 0.04 is assumed to have a morphotropic phase boundary (MPB) due to the crystal structure presenting coexistence phases between the rhombohedral and tetragonal phase. This gives the ceramic a large piezoelectric coefficient. Optimum amount of NKLNST was introduced in BNKLLT ceramics, which is one of the important factors in modifying the piezoelectric properties of the lead-free ceramics.

Table 6 Average grain, Density, T_{FA}, T_{SA}, dielectric properties, ferroelectric properties and d_{33} of (1-x)BNKLLT-xNKLNST ceramics

x	Average grain size (μm)	Measured density (g/cm^3)	Relative theoretical density (%)	T_{FA} (°C)	T_{SA} (°C)	ε_r	$tan\delta$ at T_r	ε_{SA}	$tan\delta$ at T_{SA}	P_r ($\mu C/cm^2$)	E_c kV/cm	d_{33} pC/N
0	1.52±0.29	5.69±0.04	96.7±0.84	134	338	2572	0.055	5536	0.062	35.8	22.42	210
0.02	1.36±0.26	5.76±0.6	96.6±0.71	130	334	2420	0.047	4410	0.036	28.8	17.61	232
0.04	1.38±0.28	5.78±0.05	97.2±0.65	125	330	2475	0.059	4774	0.036	28.2	14.97	266
0.06	1.41±0.33	5.73±0.07	96.9±0.64	123	323	2236	0.056	4286	0.051	15.2	12.55	131
0.08	1.43±0.36	5.68±0.09	96.0±0.73	-	-	2228	0.051	3105	0.031	11.3	11.34	95
0.10	1.47±0.39	5.59±0.08	95.3±0.79	-	-	2039	0.042	2901	0.029	5.1	12.58	48

CHARPTER V

CONCLUSION

In summary, a new binary (1-x)BNKLLT-xNKLNST lead free piezoelectric ceramics was synthesized by the solid solution combustion technique using glycine as a fuel, the x content strongly affects the phase formation and electrical response of these ceramics. The phase structure showed R+T coexist-phase of BNKLLT sample. By increment of x content $\geq$ 0.02, the phase structure of these ceramics exhibited higher tetragonality. When x was increased beyond 0.04, the phase structure started to transform into a pseudo-cubic phase. The reduction of T_{FA}, T_{SA} and the weak ferroelectric behavior of these ceramics with an increase of the x contents was observed. The resulting (1-x)BNKLLT-xNKLNST ceramics exhibited large piezoelectric coefficient of d_{33} up to 266 pC/N and near the rhombohedral-tetragonal MPB at $x = 0.04$. These results indicate that the (1-x)BNKLLT-xNKLNST ceramic is a promising candidate material for lead-free piezoelectric ceramics and a new way to modify piezoelectric behavior of BNT lead-free materials.

References

[1] E. Cross, Lead-free at last, *Nature* **432 (4)**, 24-25 (2004).

[2] G.A. Smolenskii, V.A. Isupov, A.I. Agranovskaya and N.N. Krainik, New ferroelectrics of complex composition. *Phys. Solid. State.* **2(11)**, 2651-2654 (1961).

[3] K. Rolede, J. Suchanicz and A. Kania, Time dependence of electric permittivity in $Na_{0.5}Bi_{0.5}TiO_3$ single crystals. *Ferroelectrics* **89**, 1-5 (1989).

[4]P. Bhupaijit, C. Kornphom, N. Vittayakorn and T. Bongkarn, Structural, microstructure and electrical properties of La_2O_3-doped $Bi_{0.5}(Na_{0.68}K_{0.22}Li_{0.1})_{0.5}TiO_3$ lead-free piezoelectric ceramics synthesized by the combustion technique. *Ceram. Int.* **41**, 81-86 (2015).

[5] C. Kornphom, N. Vittayakorn and T. Bongkarn, Lead-free piezoelectric ceramics based on (1- x)BNKLLT-xBCTZ binary solid solutions synthesized by the solid-state combustion technique. *J. Mater. Sci.* **51**, 4142-4149 (2016).

[6] Y.M. Li, W. Chen, J. Zhou, Q. Xu, H.J. Sun and M.S. Liao, Dielectric and ferroelectric properties of lead-free $Na_{0.5}Bi_{0.5}TiO_3$–$K_{0.5}Bi_{0.5}TiO_3$ ferroelectric ceramics. *Ceram. Int.* **31(1)**, 139-142 (2005).

[7] Z.P. Yang, Y.T. Hou, H. Pan and Y.F. Chang, Structure, microstructure and electrical properties of (1-x-y)$Bi_{0.5}Na_{0.5}TiO_3$-x$Bi_{0.5}K_{0.5}TiO_3$-y$Bi_{0.5}Li_{0.5}TiO_3$ lead-free piezoelectric ceramics. *J. Alloys. Comp.* **480**, 246-253 (2009).

[8] A. Herabut and A.M. Safari, Processing and electromechanical properties of $(Bi_{0.5}Na_{0.5})_{(1-1.5x)}La_xTiO_3$ ceramics. *J. Am. Ceram. Soc.* **80**, 2954-2958 (1997).

[9] C.R. Zhou, X.Y. Liu, W.Z. Li, C.L. Yuan and G.H. Chen, Structure and electrical properties of $Bi_{0.5}(Na, K)_{0.5}TiO_3$-$BiGaO_3$ lead-free piezoelectric ceramics. *Curr. Appl. Phys.* **10**, 93-98 (2010).

[10] P. Baettig, C.L.F Schelle, R.C. LeSar, U.V. Waghmare and N.C. A. Spaldin, Theoretical prediction of new high-performance lead-free piezoelectrics. *Chem. Mater.* **17**, 1376-1380 (2005).

[11] T. Takenaka, K.I. Maruyama and K. Sakata, $(Bi_{1/2}Na_{1/2})TiO_3$-$BaTiO_3$ system for lead-free piezoelectric ceramics. *Jpn. J. Appl. Phys.* **30**, 2236-2239 (1991).

[12] A.B. Kounga, S.T. Zhang, W. Jo, T.T. Granzow and J.G. Rödel, Morphotropic phase boundary in lead-free piezoceramics. *Appl. Phys. Lett.* **92**, 222902-9 (2008).

[13] W.J. Ji, Y.B. Chen, S.T. Zhang, B. Yang, X.N. Zhao and Q.J. Wang, Microstructure and electric properties of lead-free $0.8Bi_{1/2}Na_{1/2}TiO_3$-$0.2Bi_{1/2}K_{1/2}TiO_3$ ceramics. *Ceram. Int.* **38**, 1683-1686 (2012).

[14] Q. Gou, J.G. Wu, A.G. Li, B. Wu, D.G. Xiao and J.G. Zhu, Enhanced d_{33} value of $Bi_{0.5}Na_{0.5}TiO_3$–$(Ba_{0.85}Ca_{0.15})(Ti_{0.90}Zr_{0.10})O_3$ lead-free ceramics. *J. Alloys. Comp.* **521**, 4-7 (2012).

[15] S. Li, L. Chen, X. Ning, M. Guo and M. Zhang, $(1-x)Bi_{0.5}Na_{0.5}TiO_3$-$xK_{0.5}Na_{0.5}NbO_3$ ceramics with low coercive field: Preparation from hydrothermally synthesized precursor powders. *Ceram. Int.* **41**, 195-204 (2015).

[16] H.Q. Wang, Y.J. Dai, Z.R. Shen and X.W. Zhang, Phase transition behaviour and electrical properties of $(1-x)Bi_{0.5}Na_{0.5}TiO_3$-$x(Na_{0.53}K_{0.44}Li_{0.04})(Nb_{0.88}Sb_{0.08}Ta_{0.04})O_3$ lead-free ceramics. *J. Euro. Ceram. Soc.* **32**, 1481-1484 (2012).

[17] Y. Saito, H. Takao, T. Tani, T. Nonoyama, K. Takatori, T. Homma, T. Nagaya and M. Nakamura, Lead-free piezoceramics. *Nature* **432**, 84-87(2004).

[18] N.M. Hagh, B. Jadidian and A. Safari, Property-processing relationship in lead-free (K, Na, Li)NbO_3-solid solution system. *J. Electroceram.* **18**, 339-346 (2007).

[19] C. Wattanawikkam, N. Vittayakorn and T. Bongkarn, Low temperature fabrication of lead-free KNN-LS-BS ceramics via the combustion method. *Ceram. Int.* **39**, 399-403 (2013).

[20] C. Kornphom, N. Vittayakorn and T. Bongkarn, Low firing temperatures and high ferroelectric properties of $(Ba_{0.85}Ca_{0.15})(Ti_{0.90}Zr_{0.10})O_3$ lead-free ceramics synthesized by the combustion technique. *Ferroelectrics* **491**, 44-53 (2016).

[21] C. Kornphom, A. Laowanidwatan and T. Bongkarn, The effects of sintering temperature and content of x on phase formation, microstructure and dielectric properties of $(1-x)(Bi_{0.4871}Na_{0.4871}La_{0.0172}TiO_3)$-$x(BaZr_{0.05}Ti_{0.95}O_3)$ ceramics prepared via the combustion technique. *Ceram. Int.* **39**, 421-426 (2013).

[22] S. Yotthuan, C. Kornphom and T. Bongkarn, The effect of firing conditions on phase formation, microstructure and dielectric properties of BNKTNb-LSb ceramics prepared via the combustion technique. *Phase Transitions* **88**, 1035-1043 (2015).

[23] P. Thawong, C. Kornphom, S. Chootin and T. Bongkarn, Phase evolution and electrical properties of a new system of (1−x)[BNT–BKT–KNN]–xBCTZ lead-free piezoelectric ceramics synthesized by the solid-state combustion technique. *Phase Transitions* 89, 232-241 (2016).

[24] C. Kornphom, Combustion technique synthesis and characterization of new BNKLLT-BCTZ-NKLNST system ceramics [PhD dissertation]. *Naresuan University, Thailand*: (In progress).

[25] Y. Bai, A. Matousek, P. Tofel, V. Bijalwan, B. Nan, H. Hughes and T.W. Button, (Ba, Ca)(Zr, Ti)O_3 lead-free piezoelectric ceramics-the critical role of processing on properties. *J. Euro. Ceram. Soc.* **35**, 3445-3456 (2015).

[26] W. Jo, S. Schaab, E.A. Sapper, L. Schmitt, H.J. Kleebe, A.J. Bell and J. Rödel, On the phase identity and its thermal evolution of lead free $(Bi_{1/2}Na_{1/2})TiO_3$-6 mol%$BaTiO_3$. *J. Appl. Phys.* **110**, 074106 (2011).

[27] R. Dittmer, W. Jo, J. Daniels, S. Schaab and J. Rödel, Relaxor characteristics of morphotropic phase boundary $(Bi_{1/2}Na_{1/2})TiO_3$–$(Bi_{1/2}K_{1/2})TiO_3$ modified with $Bi(Zn_{1/2}Ti_{1/2})O_3$. *J. Am. Ceram. Soc.* **94**, 4283–4290 (2011).

[28] H. Pan, Y.T. Hou, X.L. Chao, L.L. Wei and Z.P. Yang, Microstructure and electrical properties of La_2O_3-doped $Bi_{0.5}(Na_{0.68}K_{0.22}Li_{0.1})_{0.5}TiO_3$ lead-free piezoelectric ceramics. *Curr. Appl. Phys.* **11**, 888-892 (2011).

[29] Jaffe, B., Cook, W.R. and Jaffe, H. (1971). **Piezoelectric ceramics**. India: Ceramic Book and Literature Service.

[30] Hench, L.L. and West, J. (1990). **Principles of Electronic Ceramics Hoboken.** New Jersey: John Wiley & Sons Incorporated.

[31] Haertling, H. (1999). Ferroelectric ceramics: History and Technology. **Journal American Ceramic Societies**, 82, 797.

[32] Moulson, A.J. and Herbert, J.M. (2003). **Electroceramics**. New York: Wiley- Interscience.

[33] Fousek, J. (1995). Joseph Valasek and the Discovery of Ferroelectricity. **Proceeding of the IEEE**, 1.

[34] Sawyer, C. B. and Tower, C. H. (1930). Rochelle Salt as a Dielectric. **Physics Review**, 35, 269.

[35] Jona F. and Shirane, G. (1962). **Ferroelectric crystal.** New York: Pergamum Press.

[36] Megaw, H. (1957). **Ferroelectricity in crystals.** London: Methuen.

[37] Chiang, Y. (1997). **Physical ceramics.** New York: John Wiley & Sons.

[38] Guo, R. (2000). Origin of the high piezoelectric response in $PbZr_{1/x}$ TiO_3. **Physics Review Letters**, 84, 5423.

[39] Ganguli, D. and Chatterjee, M. (1997). **Ceramic powder preparation.** USA: Kluwer Academic Publishers.

[40] Cahu, R.W., Haasen, P. and Kramer, E.J. (1996). **Materials sciences and technology**. Germany: The Federal Republic of Germany.

[41] Pierre, A.C. (1998). **Introduction to so-gel processing.** USA: Kluwer Acadamic Publishers.

[42] Ring, T.A. (1996). **Fundamentals of ceramics powder processing and synthesis**. New York: Acdemic Press Inc.

[43] Merzhanov, A.G. (1996). Combustion processes that synthesize materials. **Journal of Materials Processing Technology**, 56(1-4), 222-241.

[44] Pampuch, R. (1999). Advanced HT ceramic materials via solid combustion. **Journal of the European Ceramic Society**, 19(13-14), 2395-2404.

[45] Patil, K.C., Aruna, S.T. and Mimani, T. (2002). Combustion synthesis: An update. **Current Opinion in Solid State and Materials Science**, 6(6), 507-512.

[46] Chandradass, J., Balasubramanian, M., Bae, D.S. and Kim, K.H. (2009). Effect of different fuels on the alumina–ceria composite powders synthesized by sol–gel auto combustion method. **Journal of Alloys and Compounds**, 479(1-2), 363-367.

[47] Kopp Alves, A., Bergmann, C.P. and Berutti, F.A. (2013). **Novel synthesis and characterization of nanostructured materials**. N.P.: Springer Berlin Heidelberg.

[48] Hwang, C.C., Wu, T.Y., Wan, J. and Tsai, J.S. (2004). Development of a novel combustion synthesis method for synthesizing of ceramic oxide powders. **Materials Science and Engineering: B**, 111(1), 49-56.

[49] Patil, K.C., Aruna, S.T. and Mimani, T. (2002). Combustion synthesis: An update. **Current Opinion in Solid State and Materials Science**, 6(6), 507-512.

[50] Patil, K.C., Aruna, S.T. and Ekambaram, S. (1997). Combustion synthesis. **Solid State & Materials Science**, 2, 156-165.

[51] Aruna, S.T. and Mukasyan, A.S. (2008). Combustion synthesis and nanomaterials. **Current Opinion in Solid State and Materials Science**, 12(3-4), 44-50.

[52] Wu, K.H., Ting, T.H., Li, M.C. and Ho, W.D. (2006). Sol-gel auto-combustion synthesis of SiO_2-doped NiZn ferrite by using various fuels. **Journal of Magnetism and Magnetic Materials**, 298(1), 25-32.

[53] Suranarayana, C. and Grant Norton, M. (1998). **X-ray diffraction a practical approach**. New York: Plenum.

[54] Swartz, S.L. and Shrout, T.R. (1982). Fabrication of perovskite lead magnesium niobate. **Materials Research Bulletin,** 17(10), 1245-1250.

[55] Zuo, R., Fang, X. and Ye, C. (2007). Phase structures and electric properties of new lead $(Na_{0.5}K_{0.5})NbO_3$-$(Bi_{0.5}Na_{0.5})TiO_3$ ceramics. **Applied Physics Letter,** 90, 092904.

[56] Saito, Y., Takao, H., Tani, T., Nonoyama,T., Takatori, K., Homma,T., Nagaya, T. and Nakamura, M. (2004). Lead-free piezoceramics. **Nature,** 432, 84-87.

[57] Jiang, M., Liu, X. and Liu, C. (2010). Effect of $BiFeO_3$ additions on the dielectric and piezoelectric properties of $(K_{0.44}Na_{0.52}Li_{0.04})(Nb_{0.84}Ta_{0.1}Sb_{0.06})O_3$ ceramics. **Materials Research Bulletin,** 45, 220-223.

[58] Hagh, N.M., Jadidian, B. and Safari, A. (2007). Property-processing relationship in lead-free (K, Na, Li) NbO_3-solid solution system. **Journal of Electroceramics,** 18, 339-346.

[59] Azad, A.M., Subrmaniam, S. and Dung, T.W. (2002). On the development of high density barium metazirconate ($BaZrO_3$) ceramics. **Journal of American Ceramics Society,** 334, 118-130.

[60] Sin, A., Montaser, B. El., Odier, P. and Weiss, F. (2002). Synthesis and sintering of large batches of barium zirconate nanopowders. **Journal of American Ceramics Society,** 85, 1928-1932.

[61] Ganguli, A.K., Ahmad, T., Vaidya, S. and Ahmed, J. (2008). Microemulsion Route to the synthesis of nanoparticles. **Pure and Applied Chemistry,** 80, 2451-2477.

[62] Guillaume, B., Boschini, F., Garcia-Cano, I., Rulmont, A., Cloots, R. and Ausloos, M. (2005). Optimization of $BaZrO_3$ sintering by control of the Initial powder size distribution; a factorial design statistical analysis. **Journal of American Ceramics Society,** 25, 3593-3604.

[63] Azad, A.M. and Subramaniam, S. (2002). Temperature dependence of the dielectric response of $BaZrO_3$ by immittance spectroscopy. **Materials Research Bulletin,** 37, 11-21.

[64] Li, W., Xu, Z., Chu, R., Fu, P. and Zang, G. (2012). Enhanced ferroelectric properties in $(Ba_{1-x}Ca_x)(Ti_{0.94}Sn_{0.06})O_3$ lead-free ceramics. **Journal of European Ceramics Societies,** 32, 517-520.

[65] Sumang, R., Wicheanrat, C., Bongkarn, T. and Maensiri, S. (2015). High densification and dielectric properties of lead-free $(K_{0.5}Na_{0.5})NbO_3$ piezoelectric ceramics with optimum excess Na_2O and K_2O contents. **Ceramics International,** 41, S136-S142.

[66] **Science Lab Center**. (2004). Retrieved February 1, 2014, from http://www.sci.nu.ac.th/slcs/index.php.

[67] Ronald, E.L. (2010). **Characteization of ceramics**. New York: Momentum.